

POLITECNICO DI TORINO

Collegio di Ingegneria Chimica e dei Materiali

**Corso di Laurea Magistrale
in Ingegneria dei Materiali
Tesi di Laurea Magistrale**

**Correlazioni nanostruttura - proprietà meccaniche
del PEEK e sua integrazione in laminati con
applicazione in ambito aerospaziale**



Relatore

firma del relatore (dei relatori)

Prof. Marco Sangermano

Dr. Araceli Flores

Patricia Enrique Jimenez

Candidato

Matteo Malacarne

Settembre 2018

Correlazioni nanostruttura - proprietà meccaniche del PEEK e sua integrazione in laminati con applicazione in ambito aerospaziale

Introduzione

I polimeri sono materiali leggeri che possono essere lavorati e stampati a costi relativamente bassi e questi importanti vantaggi hanno favorito la loro progressiva incorporazione nella vita quotidiana, sostituendo i metalli in molte applicazioni. In particolare, i polimeri ad alte prestazioni presentano eccellenti proprietà meccaniche ad alte temperature. Questa tipologia di polimeri ha trovato applicazione nell'industria aeronautica e aerospaziale perché la loro bassa densità consente di risparmiare sui costi del carburante. Il polietereterchitone (PEEK) è uno dei più importanti polimeri ad alte prestazioni. È un materiale rigido, opaco, noto per la sua combinazione unica di proprietà, che include una eccezionale resistenza chimica, all'usura, un buon comportamento ad elevate temperature e una buona stabilità dimensionale. Il PEEK è disponibile in diversi formati a seconda dell'applicazione e del metodo di elaborazione. I componenti in PEEK sono utilizzati in diversi campi: da automobili, aeromobili, pompe industriali, valvole e guarnizioni, a supporti di wafer di silicio, connettori e strumenti chirurgici sterilizzabili e in campo medico.

La ricerca sui materiali a base di PEEK è molto attiva ormai fin dagli inizi degli anni '80 del secolo scorso. Molte parti della nuova generazione di velivoli sono costituite da PEEK al fine di rendere gli aerei più leggeri, con l'obiettivo di ridurre le emissioni di CO₂ e il consumo di carburante. Inoltre, il PEEK mostra una buona stabilità termica: la temperatura di pirolisi è di circa 550 ° C, il punto di fusione è 343 ° C e la temperatura di transizione vetrosa è 145 °C. Questo intervallo di temperature è particolarmente elevato per un materiale polimerico. Inoltre, ha un buon comportamento in ambienti corrosivi, infatti è insolubile in tutti i comuni solventi, ad eccezione di acidi forti come il 98% di acido solforico e questo è il motivo principale per cui viene utilizzato nel sistema di tubazioni degli aerei.

Al fine di espandere i limiti di prestazione di PEEK, è abbastanza comune rinforzarlo con uno filler che dà origine a un materiale composito. Ad esempio, nel settore aerospaziale, il PEEK è

soltamente rinforzato con fibre di carbonio ad alta resistenza per componenti strutturali o prefabbricati. I materiali compositi sono molto comuni al giorno d'oggi e trovano molte applicazioni in tutti i campi industriali. L'idea alla base è combinare le proprietà dei due materiali di partenza per produrne un nuovo materiale con proprietà migliorate. Ad esempio, la combinazione di un polimero con fibra di carbonio può produrre un materiale leggero con proprietà meccaniche superiori.

È interessante notare che Victrex, una società che produce PEEK per applicazioni aerospaziali, segnala un numero crescente di parti metalliche sostituite dai compositi PEEK perché, nonostante il fatto che entrambi i materiali presentino prestazioni meccaniche simili, il composito è significativamente più leggeri e questo consente un risparmio di 10000 \$ in costi di carburante annuali. Il composito PEEK è ignifugo, caratteristica importante per i componenti di un aereo. Attualmente il composito più comune di PEEK è 90HMF40.

Un comune composito utilizzato in industria aeronautica consiste in strati alternati di una matrice polimerica con fibre di vetro o con fibre di carbonio. Le proprietà meccaniche di tali sistemi multilaminari possono essere facilmente ottimizzate e di solito le proprietà interlaminari limitano le prestazioni meccaniche complessive del composito. Il legame interfacciale tra matrice e le fibre gioca un ruolo fondamentale e, quindi, l'interfase appare come un punto critico da ottimizzare. Recenti studi hanno evidenziato che le proprietà meccaniche dell'interfase tra le fibre di vetro e il PEEK nei sistemi multilaminari possono essere migliorate aggiungendo nanofiller carboniosi come i nanotubi di carbonio.

In questa tesi, viene studiato un sistema multilaminare di matrice PEEK e con filler di fibra di carbonio, il tutto rinforzato con grafene. Quest'ultimo viene incorporato nello strato polimerico con un duplice scopo. Da un lato, si prevede che il grafene migliori le proprietà meccaniche dello strato polimerico dall'altro, si prevede la formazione di un'interfase tra la matrice e le fibre di carbonio.

Il lavoro è quindi diviso in tre parti. In primo luogo, viene eseguita la caratterizzazione meccanica di film PEEK mediante indentazione (si ottengono valori di durezza e modulo) e si confrontano le proprietà meccaniche ottenute con la nanostruttura. Per chiarire tale relazione, viene utilizzata una gamma di temperature di lavorazione, dando origine a diverse proprietà meccaniche e nanostrutture. Nella seconda fase, viene esplorata l'influenza rinforzante del grafene sulle proprietà meccaniche e sulla nanostruttura di PEEK.

Infine, vengono studiate le proprietà meccaniche dei sistemi multilaminari di matrice PEEK con filler di fibra di carbonio rinforzato con grafene, con particolare enfasi sulla possibile comparsa di un'interfase tra le fibre e lo strato a base polimerica.

Materiale e metodo

Nel seguente capitolo verranno presentati i materiali e i metodi utilizzati durante la fase sperimentale con accenni agli step intermedi che porteranno all'ottenimento degli esiti finali sintetizzati nel capitolo risultati.

Il lavoro sperimentale, basato sull'analisi della micro e nanostruttura del PEEK, inizia con la formazione di film amorfì in PEEK. La matrice utilizzata è poli (etero etere chetone) in polvere con un peso molecolare medio di 40.000 g/mol (PEEK 150P) fornito da Victrex, Regno Unito. Questo materiale è stato sottoposto ad un processo di essiccazione per una settimana al fine di eliminare tutta l'acqua presente all'interno.

Le polveri di PEEK sono raffigurate nella seguente figura.

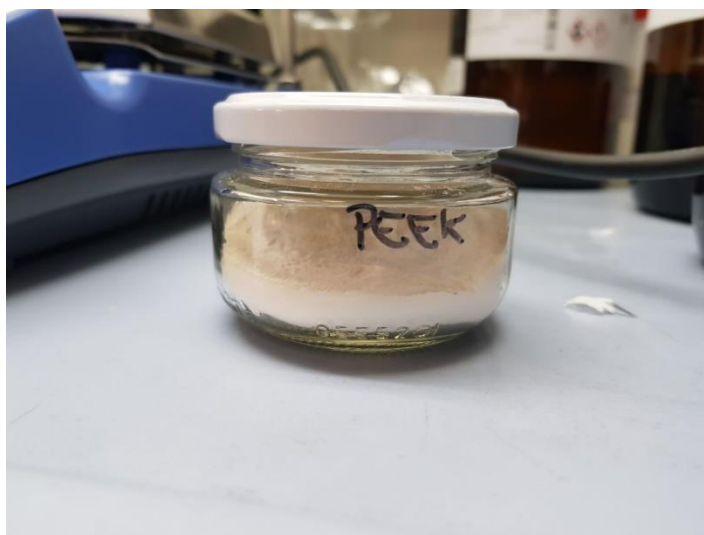


Figura 1. Polveri essicate di PEEK

Queste vengono depositate su un film di UPILEX, poliimmide, precedentemente pulito con alcool. Si è utilizzato l'UPILEX poiché ha una temperatura di fusione superiore a 343°C e perchè permette una facile rimozione del film amorfico di PEEK. L'esperimento prevede di porre le polveri di PEEK tra due pellicole di UPILEX e posizionare il tutto su una piastra riscaldante. Si è utilizzato un termometro per tenere sotto controllo la temperatura del porta campione e della piastra. Quest'ultima risulta avere una temperatura superiore rispetto a quella del porta campione a causa dell'inerzia termica. Inoltre, per facilitare la fusione delle polveri di PEEK,

si è utilizzato un peso di 5 Kg perché favorisce il contatto tra il campione e la piastra riscaldante. Una volta ottenuta la fusione completa delle polveri, il PEEK è stato sottoposto a un processo di raffreddamento. I metodi utilizzati sono due: raffreddamento in acqua con ghiaccio o in azoto liquido. Il primo si è rivelato più efficace rispetto al secondo. L'utilizzo dell'azoto liquido, infatti, non ha portato alla formazione di un campione amorfico, probabilmente perché il gradiente di temperatura tra azoto liquido e campione era troppo elevato: una pellicola di vapore si è sviluppata tra il liquido e il campione per un tempo sufficiente da permettere la cristallizzazione di quest'ultimo.

I campioni posti in acqua e ghiaccio invece, risultano avere un aspetto trasparente, tipico di un materiale amorfico. I campioni ottenuti e successivamente analizzati sono denominati Hy_A2 e Hy_A4. Essi sono stati sottoposti a una analisi ai raggi X per determinare la loro struttura cristallina. L'interazione tra i raggi X e il materiale genera un fenomeno fisico chiamato pattern di diffrazione. La tecnica utilizzata è chiamata WAXS, scattering a raggi X grandangolare. Il generatore anodico rotante Micro Star che funziona a 100 mA e 50 kV è rappresentato nella figura 2.

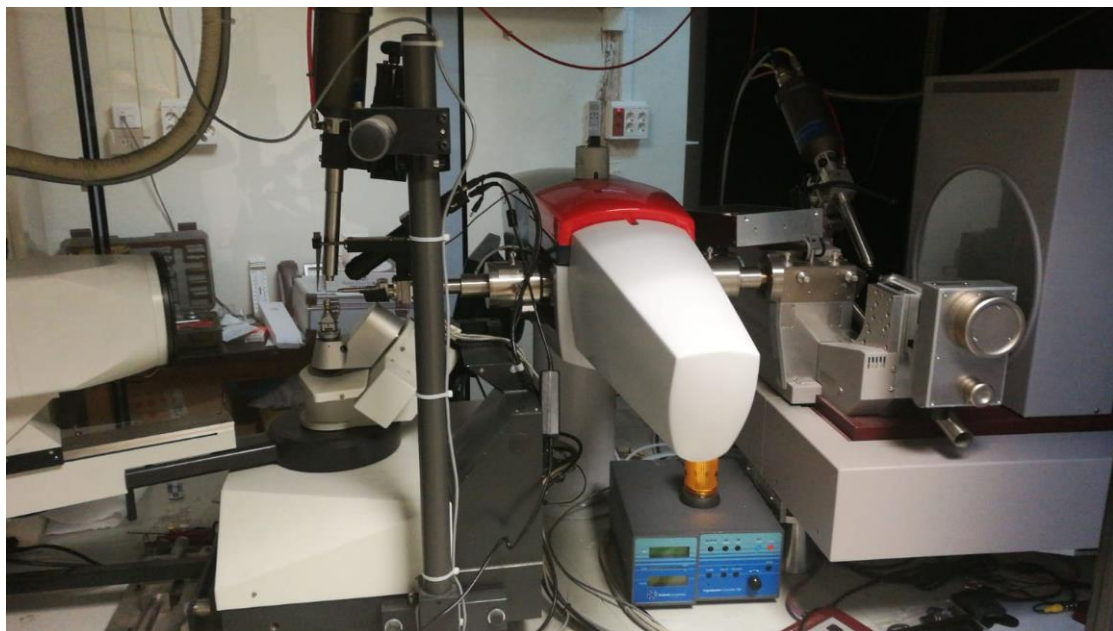


Figura 2. Micro Star

La risoluzione ottenuta è pari a 3450x3450 pixel e 100 μm / pixel. Per fare l'esperimento, la lunghezza d'onda utilizzata è pari a $\lambda = 0,1542 \text{ nm}$ e la distanza tra il campione e il rivelatore è di 220 mm. I pattern di diffrazione e i dati ottenuti dai raggi X vengono corretti, sviluppati e integrati usando il software FIT2D per creare grafici che rappresentano l'intensità (asse y) in

funzione dell'angolo di diffrazione 2θ (asse x). Inoltre, viene utilizzato il software Peakfit v4.12 per determinare il grado di cristallinità con due diverse funzioni: Pearson VII per i picchi cristallini, Asym Dbt per le regioni amorfe.

I pattern di diffrazione dei campioni Hy_A2 e Hy_A4 risultano essere molto simili: non presentano linee, ma un alone nero come è possibile osservare nella figura 3.

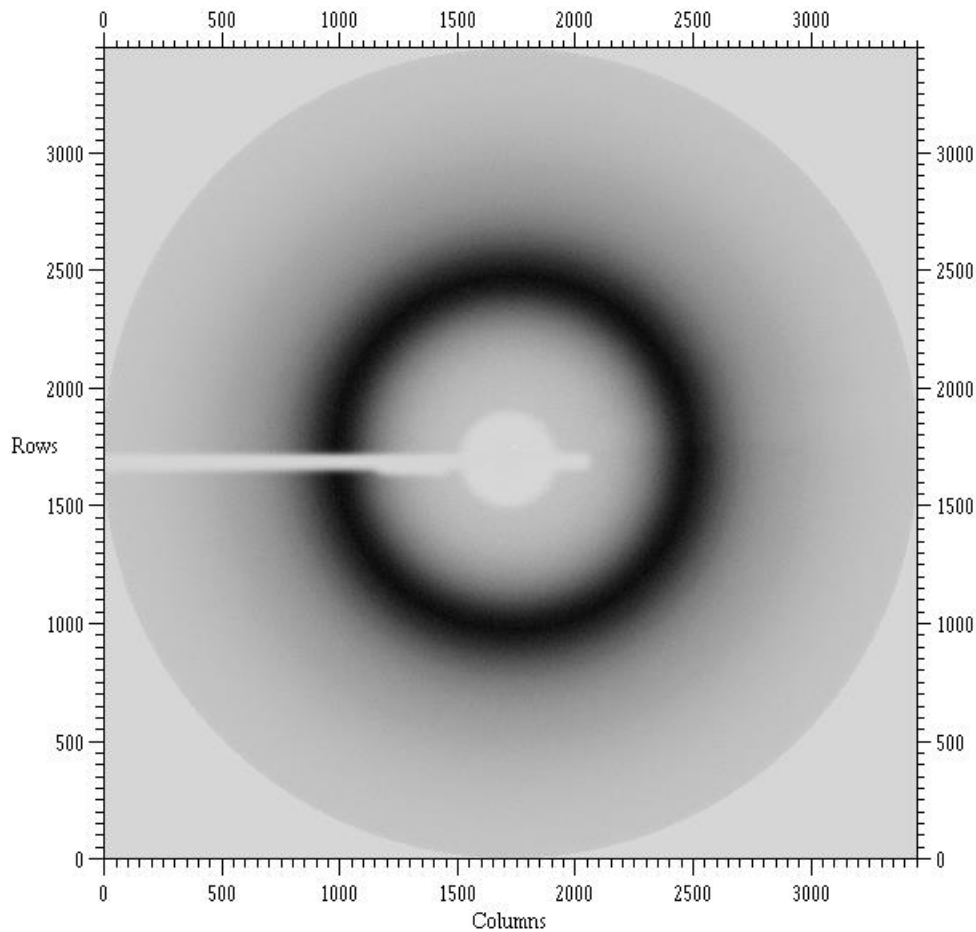


Figura 3. Pattern di diffrazione di PEEK amoro

Dopo l'analisi con i software precedentemente descritti, il grado di cristallinità risulta essere pari all'1% per entrambi i campioni. A partire da questi film di PEEK, si creeranno i campioni che saranno sottoposti a un processo di cold crystallization: tecnica che porta il campione da temperatura ambiente a una temperatura di almeno dieci gradi superiore a quella di transizione vetrosa per effettuare un processo di cristallizzazione.

I campioni vengono sottoposti a temperature differenti per analizzare la variazione del grado di cristallinità in base alla temperatura. Tuttavia, prima di eseguire la cold crystallization, è stata effettuata la calibrazione dello strumento utilizzato per il processo. Per calibrare la Linkam, rappresentata nella seguente immagine, sono stati utilizzati degli elementi con una temperatura

di fusione nota poiché la temperatura mostrata dall'apparecchio non corrisponde effettivamente alla temperatura della piastra riscaldata.



Figura 4. Linkam

Il Salophen, materiale in polvere utilizzato per calibrare lo strumento, ha una temperatura di fusione pari a 191°C ma fonde quando la macchina risulta essere a 213.5°C. L'aumento di temperatura è impostato a 10 °C/min e una volta raggiunta la teorica temperatura di fusione del campione, aumenta di 1°C/min così da diminuire il più possibile l'effetto dell'inerzia termica. È stato utilizzato lo stesso metodo per altri materiali quali 1-Hesacosanol, Benzanilid e il Tetracosanol. Facendo una interpolazione lineare tra le temperature teoriche di fusione e quelle ottenute si è in grado di prevedere a quale temperatura si debba impostare allo strumento.

I limiti di temperatura adottati per la cold-crystallization sono 240°C come massimo mentre 145°C come minimo. Grazie a questo ampio range di temperature sono riuscito ad ottenere diversi campioni con diversi gradi di cristallinità.

Un fatto interessante è il seguente: la modalità con cui si stringono i campioni tra i portacampioni durante la cold-crystallization influisce non solo sulle proprietà meccaniche ma anche sul grado di cristallinità e sull'orientamento preferenziale. Più è compresso il campione, più è favorito il contatto tra quest'ultimo e il portacampione e più si impone la formazione di orientamenti preferenziali. Per questi motivi molti esperimenti sono stati ripetuti cercando di stringere il meno possibile in modo tale da non formare orientamenti preferenziali nei campioni.

Come è stato detto nell'introduzione l'obiettivo principale di questo lavoro sperimentale è correlare la nanostruttura con le proprietà meccaniche. Queste ultime sono studiate con un nanoindentatore G300, tuttavia sono necessarie delle operazioni per preparare i campioni poiché la dimensione dell'indentazione è dell'ordine di grandezza sia micrometrico che nanometrico. Per minimizzare la rugosità superficiale sono necessari diversi step di lucidatura. Inizialmente, i campioni vengono posizionati verticalmente in un portacampione di plastica che successivamente verrà incollato su uno stampo in cui sarà versata una soluzione di resina epossidica. Il tutto viene lasciato seccare per un giorno. I campioni vengono portati in rilievo grazie a uno strumento chiamato "Microtome" che taglia ad ogni ciclo 4 micron di materiale. Per essere certi che i campioni siano in superficie, è necessario osservare che i film di resina epossidica tagliati contengano un numero di "tagli" uguali al numero dei campioni. Oltre a questi step iniziali, sono necessari altri step di lucidatura che prevedono l'utilizzo di una macchina chiamata "Polish Machine" che utilizza delle carte in carburo di silicio con rugosità progressivamente più fine. La prima carta utilizzata è denominata P1200 e il tempo di lucidatura è fissato a 4 minuti. La seconda è chiamata P1500 e il tempo di processo è di 4 minuti e 30 secondi. Per gli ultimi due step sono stati utilizzati P2500 e P4000 per 5 minuti l'uno. Per concludere la lucidatura si è soliti utilizzare un microcloth con allumina per rendere la superficie più liscia e brillante.

In seguito allo step di lucidatura, i campioni sono pronti per essere sottoposti al processo di nanoindentazione.

Per indentazione si intende la continua misura dello spostamento della punta, indentatore, in funzione della forza applicata. La nanoindentazione utilizza indentatori di dimensioni nanometriche, in questo caso è utilizzata una punta denominata Berkovich, che ha una forma piramidale a tre lati. Per quanto riguarda i materiali polimerici, che presentano un

comportamento viscoelastico, l'analisi della durezza e del modulo elastico (E) sono effettuate utilizzando la tecnica denominata “Analisi meccanica dinamica” che in inglese corrisponde a “Continuous stiffness measurement”. Questo test sovrappone al carico applicato sul materiale un'oscillazione di piccola ampiezza. Il tipico ciclo carico-scarico è rappresentato dal seguente grafico.

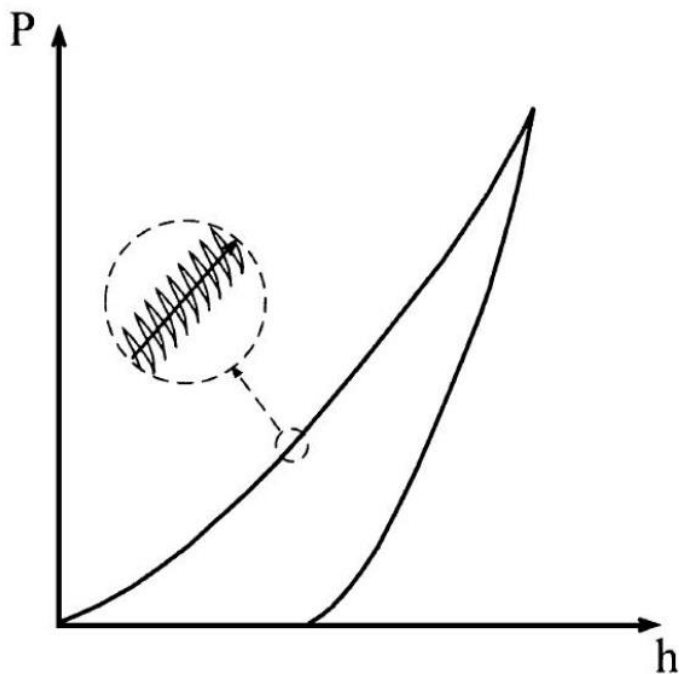


Figura 5. Curva ottenuta con tecnica CSM

La durezza può essere definita, per un materiale semicristallino, come la resistenza alla deformazione plastica derivante da un volume di materiale che ha determinate proprietà nanometriche. Prima di eseguire l'esperimento è necessario calibrare lo strumento, in particolare la punta. La taratura dell'area della punta di solito consiste nell'effettuare una serie di indentazioni su un materiale che va incontro a pile-up, come per esempio la silice fusa, e dove E e H sono indipendenti dalla dimensione dell'indentazione.

Inoltre, si deve prestare particolare attenzione alla temperatura a cui viene eseguito l'esperimento: svolgendo analisi a livelli nanometrici piccoli cambi di temperatura possono generare espansione o compressione termica che possono influire sui risultati ottenuti.

Laminati in PEEK

Il PEEK è un materiale termoplastico che come ho già precisato sopra ha delle ottime proprietà meccaniche. Se combinato con filler quali il grafene o fibre di carbonio può migliorare ulteriormente le sue proprietà meccaniche. L'utilizzo della fibra di carbonio, disposta a 0° e a 90° nella matrice polimerica, porta alla formazione di un composito che risulta avere una durezza e un modulo E' di gran lunga superiore rispetto ai materiali semicristallini. I materiali compositi analizzati sono 3 e li ho denominati nel seguente modo:

- PEEK_CF1: PEEK che contiene 10 strati di polimero e 9 di fibra di carbonio
- 5GsPEEK: PEEK film con 5% di grafene e 5% di PEEK solfonato.
- PEEK_CF3Gs: PEEK con fibre di carbonio e con un 5% di grafene e 5% di PEEK solfonato in grado di garantire una buona adesione tra PEEK e grafene.

Il secondo materiale è un film di PEEK con il 5% in peso di grafene e 5% di PEEK solfonato: quest'ultimo ha la capacità di aiutare l'adesione tra matrice e filler. Il composito ha uno spessore di 480 μm , può quindi essere analizzato ai raggi X.

Risultati

In questo capitolo conclusivo sono esposti i risultati del lavoro sperimentale mostrando inizialmente i campioni ottenuti dalla cold crystallization e successivamente le loro proprietà meccaniche confrontandole con la nanostruttura.

La cold crystallization ha portato all'ottenimento di diversi campioni di PEEK con diversi gradi di cristallinità. La seguente tabella riassume i risultati ottenuti mostrando i campioni analizzati, le temperature e il tempo a cui sono stati sottoposti.

Tabella 1. Campioni di PEEK ottenuti per cold crystallization

Campioni	Temperatura teorica (°C)	Temperatura reale(°C)	Tempo (min)
PEEK166.1h	166	190	60
PEEK150.1h	150	171	60
PEEK156.12h	156	178	720
PEEK175.1h	175	20	60
PEEK220.1h	220	251	60
PEEK166.12h	166	190	720
PEEK166.1hNEW	166	190	60
PEEK240.1h	240	274	60
PEEK156.1h	156	178	60
PEEK185.1h	185	212	60
PEEK160.1h	160	183	60
PEEK240.1hN	240	274	60
PEEK145.1h	145	166	60

Questi campioni sono stati nuovamente analizzati ai raggi X con la tecnica WAXS, sempre con l'obiettivo di determinare la loro struttura cristallina utilizzando un metodo non distruttivo.

Si ottengono differenti spettri di diffrazione. Il materiale con il grado di cristallinità più basso, pari al 4% ha il seguente spettro di diffrazione.

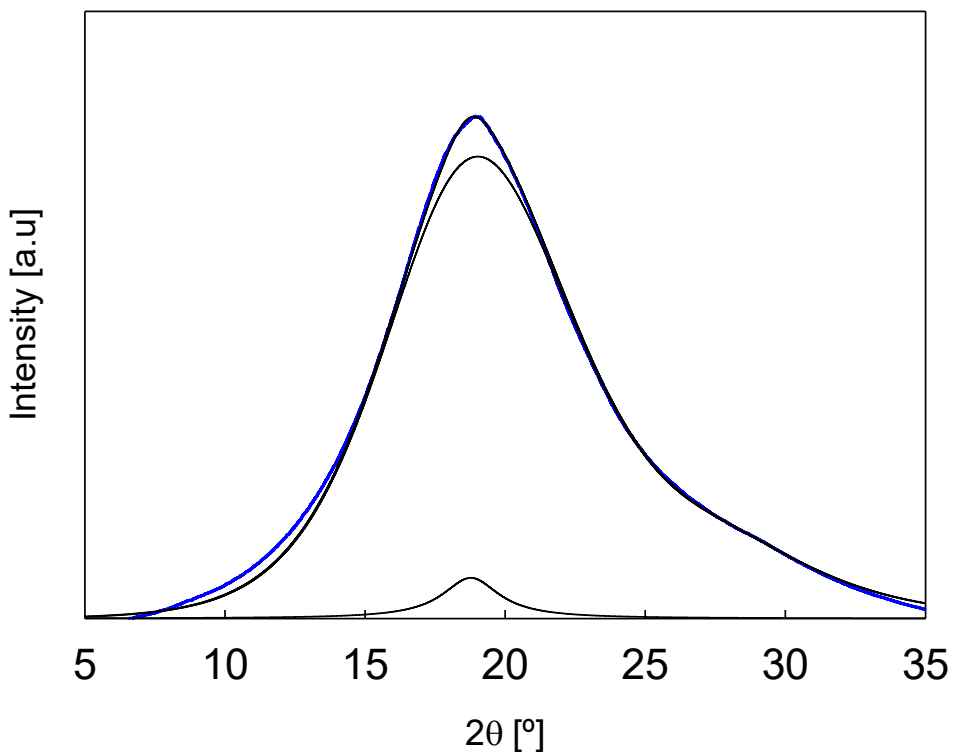


Figura 6. Spettro di diffrazione PEEK145.1h

Il picco presente circa a 18° rappresenta la parte cristallina che in questo caso corrisponde a circa al 4%.

La successiva figura rappresenta invece lo spettro di diffrazione del PEEK185.1h in cui sono evidenziati tutti i piani di diffrazione e i relativi angoli di diffrazione. Il picco più intenso appartiene al piano (110) che corrisponde a un angolo di 18.88° . A 26° esiste il piano (112) poco visibile in questi campioni ma molto evidente con il campione di PEEK con grafene che si analizzerà in seguito. La seguente figura mostra i piani di diffrazione caratteristici del PEEK in funzione dell'angolo.

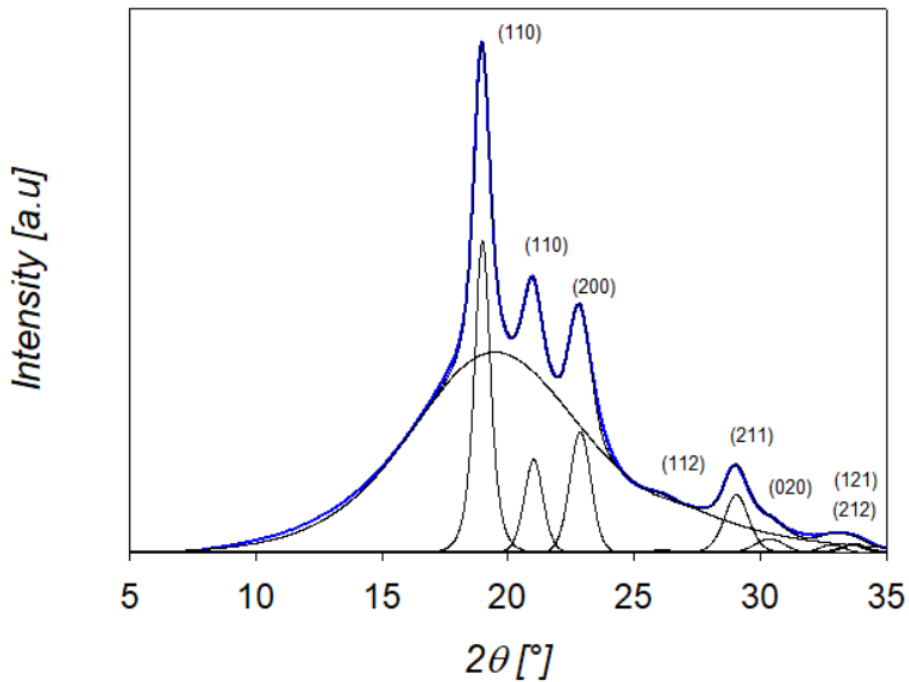


Figura 7. Spettro di diffrazione PEEK185.1h con relativi piani di diffrazione

Una volta ottenuto informazioni sulle caratteristiche nanometriche dei campioni, questi vengono analizzati con un nanoindentatore.

Grazie a questo strumento si è in grado di confrontare i valori delle proprietà meccaniche con la nanostruttura dei campioni e si è in grado di valutare l'effetto del grafene su di essi.

Le proprietà meccaniche dei campioni di PEEK con diversi gradi di cristallinità sono riassunte nella seguente tabella.

Tabella 2. Proprietà meccaniche, orientazioni preferenziali e cristallinità dei differenti campioni

Campioni	Piani preferenziali	Grado di cristallinità	E' (GPa)	H (MPa)
Campioni isotropici				
PEEK150.1h	-	9%	3.84 ± 0.06	264 ± 7
PEEK156.1h	-	12%	3.88 ± 0.05	271 ± 5

PEEK240.1h	-	26%	4.44 ± 0.03	332 ± 6
PEEK160.1h	-	16.5%	3.79 ± 0.08	263 ± 9
PEEK185.1h	-	19.5%	4.27 ± 0.08	312 ± 6
PEEK166.1hN	-	17.5%	4.12 ± 0.05	294 ± 6
PEEK145.1h	-	4%	3.28 ± 0.05	201 ± 7
PEEK240.1hN	-	25%	4.27 ± 0.04	307 ± 9
Campioni con orientazioni preferenziali				
PEEK166.1h	(110) (200) (211)	21%	4.26 ± 0.03	306 ± 5
PEEK156.12h	(110)	19%	4.11 ± 0.06	297 ± 5
PEEK220.1h	(110) (200)	24%	4.39 ± 0.06	329 ± 8
PEEK166.12h	(110) (200)	20.5%	4.21 ± 0.07	309 ± 8
PEEK175.1h	(110)	20%	4.18 ± 0.05	305 ± 6

Si osserva che con l'aumento del grado di cristallinità le proprietà meccaniche (E' e H) aumentano di conseguenza. Il massimo grado di cristallinità ottenuto mediante la tecnica della cold crystallization è pari al 26%.

Dalla precedente tabella si può inoltre osservare come gli orientamenti preferenziali non influiscano sulle proprietà meccaniche del campione.

Il seguente grafico conferma ancora una volta la corrispondenza tra grado di cristallinità e durezza. I punti rossi mostrano i campioni di PEEK con orientamenti preferenziali mentre quelli in nero rappresentano quelli isotropici.

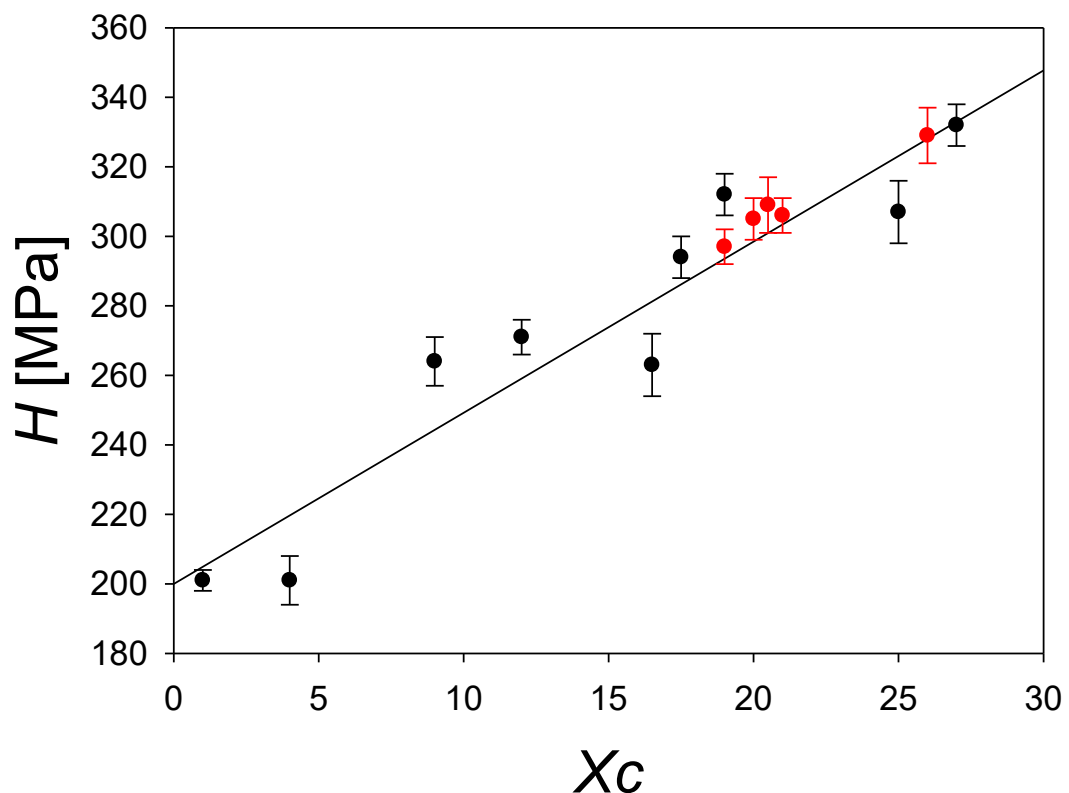


Figura 8. Durezza vs grado di cristallinità

Per quanto riguarda invece i materiali compositi, si sono effettuate due analisi con il nanoindentatore. Con il primo esperimento abbiamo potuto constatare l'effetto del grafene sul PEEK. Si sono effettuate delle indentazioni sia nelle zone periferiche del campione sia internamente, tra strati di fibre, in modo tale da avere un risultato il più prossimo possibile alla realtà. Con i seguenti due grafici è possibile osservare quanto influisca il grafene sul modulo e sulla durezza. Il punto verde rappresenta il film di PEEK con grafene. Si può constatare che il modulo aumenta di 1.5 GPa mentre la durezza aumenta di 80 MPa rispetto al valore standard.

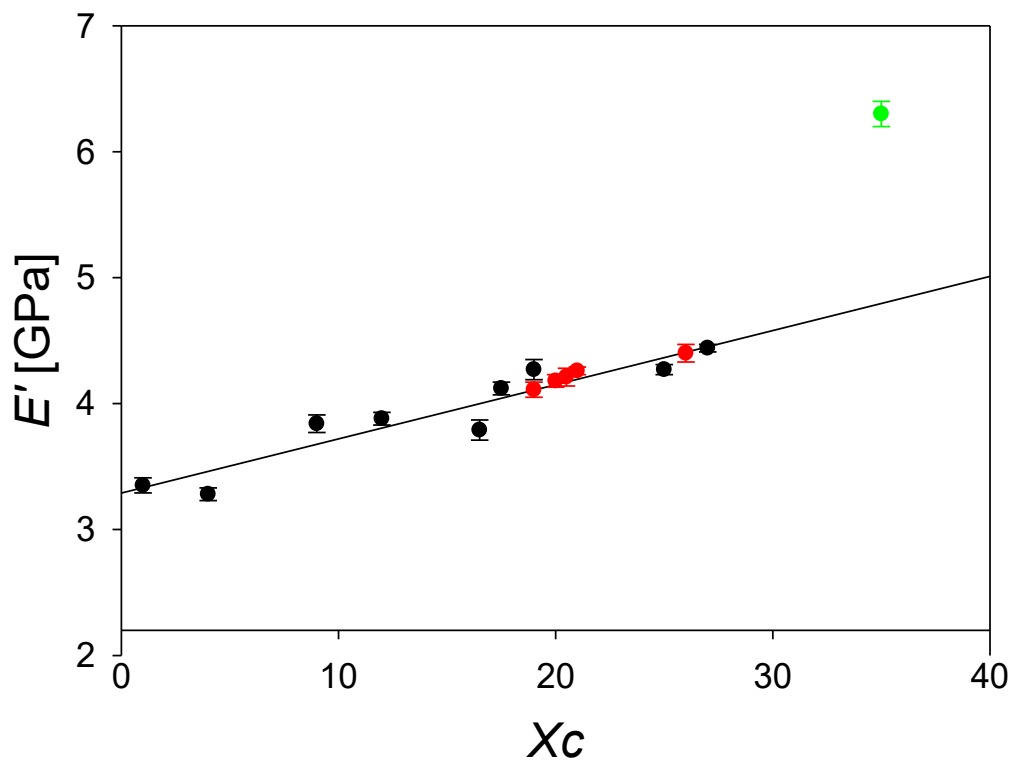


Figura 9. Confronto proprietà meccaniche tra PEEK semicristallini e film di PEEK con grafene

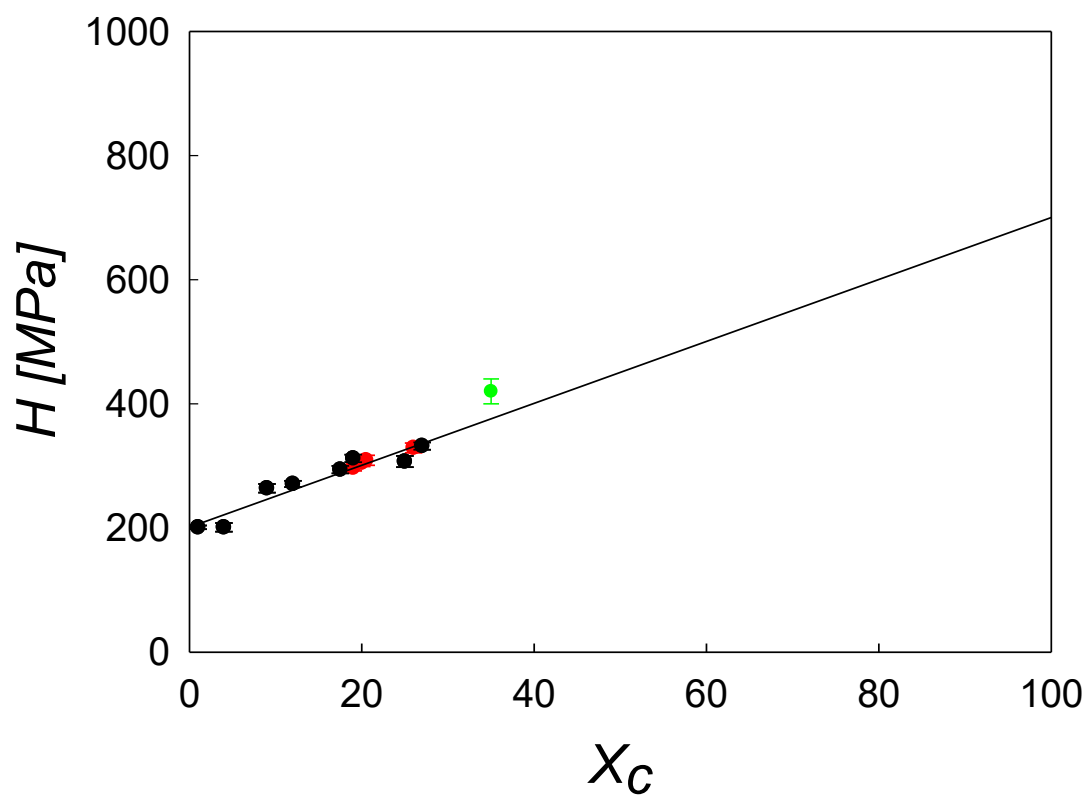


Figura 10. Confronto proprietà meccaniche tra PEEK semicristallini e film di PEEK con grafene

Con il secondo metodo si è invece studiata l'eventuale presenza di interfacce tra matrice e fibre di carbonio con e senza grafene. Si è svolta una analisi di tipo lineare su una singola fibra. In questo esperimento la profondità di indentazione è pari a 50nm. Si sono effettuati circa 60 impronte distanziate l'una dall'altra di circa 0,5 micron. I risultati ottenuti sono raffigurati nelle figure 40-41-42-43, presenti nella trattazione sperimentale. Un esempio di grafico è il seguente.

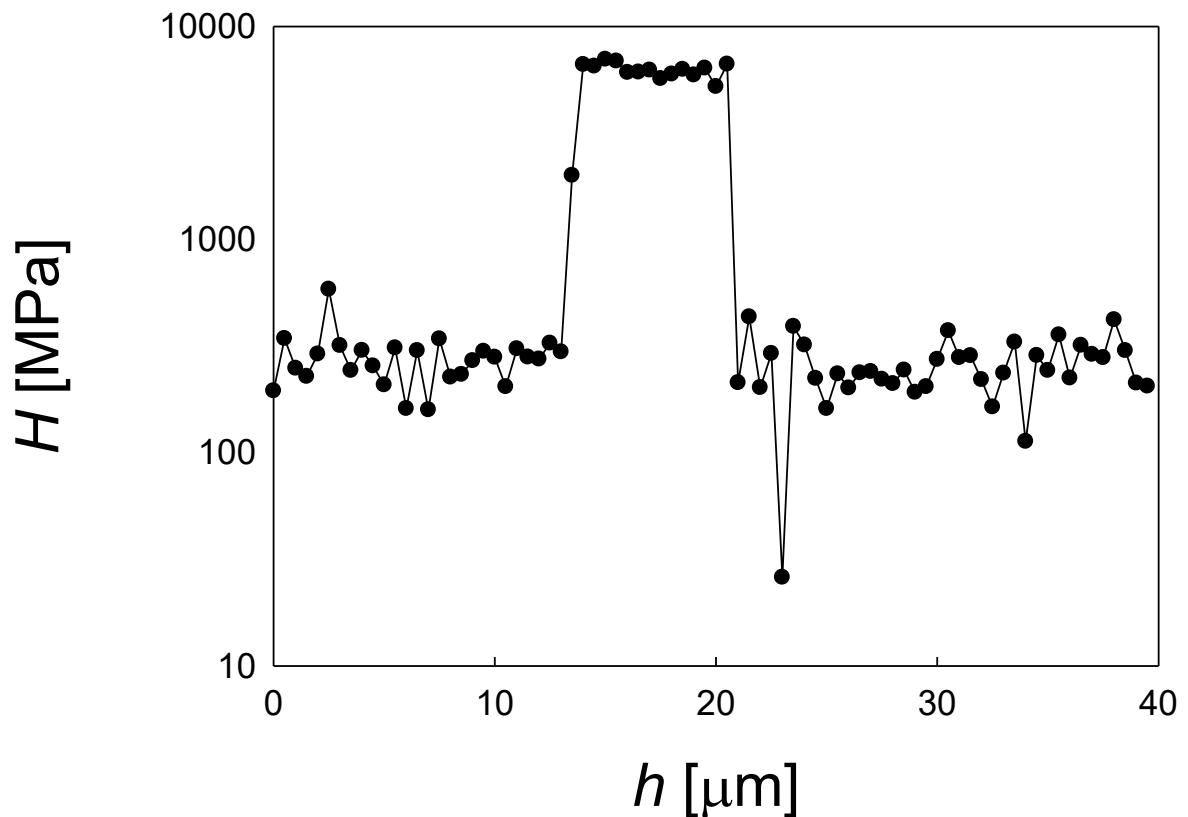


Figura 11. Analisi lineare per valutare l'esistenza di interfasi

Si può notare come i valori cambino drasticamente quando si indenta il polimero e la fibra. Tuttavia, il polimero risulta essere rinforzato ovvero avere un modulo e una durezza intorno a $5,07 \pm 0.04$ GPa e 370 ± 12 MPa per il campione PEEK_CF1 e $H=410 \pm 20$ MPa e $E'=6.6 \pm 0.3$ GPa per il PEEK_CF3Gs. Si può notare come l'aggiunta di grafene, anche se in piccole quantità (5% in peso), aumenta ulteriormente le proprietà meccaniche del composito. Da questi grafici risulta che il grafene non aiuti a migliorare il contatto tra fibra di carbonio e PEEK e quindi a

diminuire il rischio di frattura interlaminare perché non vi è un aumento progressivo delle proprietà meccaniche in prossimità della fibra.

Conclusione

È stato dimostrato che il PEEK quasi amorfico può essere trasformato in un materiale semicristallino mediante ricottura a temperature nell'intervallo di 145 e 240 °C. Aumentando la temperatura di cristallizzazione, il grado di cristallinità aumenta e vi è un aumento simultaneo di modulo e durezza. Si trova una relazione lineare tra durezza (o modulo) con il grado di cristallinità. Inoltre, si è riscontrato che i cambiamenti della dimensione dei cristalli lamellari non hanno alcun effetto rilevante sulle proprietà meccaniche.

L'incorporazione del grafene produce un notevole aumento delle proprietà meccaniche. L'analisi di H ed E' in funzione dello spostamento suggerisce che il grafene è ben disperso nella matrice PEEK in scala micrometrica. L'analisi dei dati, sulla base delle precedenti correlazioni stabilite tra H (ed E') e cristallinità, rivela che le modifiche nanostrutturali prodotte sul PEEK dall'incorporazione del grafene non influenzano significativamente le proprietà meccaniche. Quindi, il rinforzo principale è dovuto alle proprietà intrinseche del filler.

Per quanto riguarda il sistema multilaminare, i risultati non hanno dimostrato l'esistenza di una interfase, né nello strato polimerico privo di grafene, né in quello rinforzato con il filler. Una mappatura di H ed E' attraverso l'interfaccia tra fibra e matrice non mostrava un apparente aumento delle proprietà meccaniche quando la misura veniva effettuata in prossimità della fibra.

In sintesi, è stato trovato che il grafene aumenta la durezza e il modulo del PEEK. Tuttavia, non sembra migliorare l'interfase con le fibre di carbonio e quindi non ci si aspetta che l'adesione tra di esse sia migliorata. Quindi, l'incorporazione di grafene ben disperso non è sufficiente per risolvere il problema del fallimento interlaminare. L'utilizzo di una quantità maggiore di grafene non sembra un'alternativa adatta perché il filler è troppo costoso e perché si rischia una possibile agglomerazione. Il lavoro futuro dovrebbe prendere in considerazione altri approcci come la modifica della superficie delle fibre di carbonio per aumentare la bagnabilità.

Thesis approach and justification

The thesis “Nanostructure correlations - mechanical properties of PEEK and its integration in laminates with aerospace application” is the product of a personal interest in the field of polymeric materials and of my whole university path, started at the Politecnico of Turin and ended in Madrid at the Universidad Politecnica.

As a material engineer, during my degree, I had developed a deep curiosity in that field. In Madrid I had the opportunity to work for six months in a laboratory putting into practice the theoretical knowledge that I built.

There are mainly three important reasons behind the elaboration of the following study.

The first one is an interest in experimental study of the mechanical properties of a material and in the chemical and physical properties’ changes once subjected to crystallization. The second one is an interest about the use of polymeric materials more eco-friendly in structural applications in order to replace metallic materials. Finally, I wanted to observe those phenomena, studied at the University, in a practical way.

Index

<i>Thesis approach and justification</i>	20
1. Introduction	22
2. Materials and methods	24
2.1 Materials	24
2.1.1 Experiment	24
2.1.2 Calibration	28
2.1.3 Cold Crystallization	29
2.1.4 Preparation of samples	31
2.1.5 Composite Materials	33
2.2 Methods	35
2.2.1 X-ray analysis, material characterization	35
2.2.1.1 Lateral crystal size determination	39
2.2.2 Mechanical properties from nanoindentation: correlation with nanostructure ..	41
2.2.2.1 Introduction to nanoindentation	41
2.2.2.2 Oliver-Pharr method	41
2.2.2.3 Application to polymers: Continuous Stiffness Measurement (CSM)	43
2.2.2.4 The indenter	45
2.2.2.5 Correlation of hardness and Young modulus with nanostructure	46
3. Results and discussion	48
3.1 PEEK	48
3.1.1 Nanostructure by means of the X-ray diffraction	48
3.1.2 Mechanical properties from nanoindentation	57
3.1.3 Correlation mechanical properties-crystallinity	59
3.2 Composites materials	63
3.2.1 Influence of graphene on PEEK properties	63
3.2.2 Composites properties	67
4. Conclusions	73
5. Bibliography	74

1. Introduction

Polymers are lightweight materials that can be processed and molded at relatively low costs and these important advantages have promoted their progressive incorporation into the daily life, substituting metals in many applications. In particular, high performance polymers exhibit excellent mechanical properties at high temperatures. This type of polymers has found niche of application in the aeronautical and aerospace industry because their low density allows saving fuel costs. Poly(ether ether ketone) (PEEK) is one of the most important high performance polymers. It is a rigid, opaque material known for its unique combination of properties, which includes exceptional chemical, wear, electrical and temperature resistance, as well as dimensional stability. PEEK is available in many different grades and formats depending on the application and on the processing method. [1] PEEK components are used in several fields: from cars, aircrafts, industrial pumps, valves and seals, to silicon wafer carriers, connectors and sterilisable surgical instruments and in the medical field. [4]

Research on PEEK-based materials has been very active since it was first synthesized in the early 80's of the last century. Many parts of the new generation of aircrafts are constituted by PEEK in order to create lighter planes, aiming to decrease the CO₂ emissions and the fuel's consumption. [4] PEEK exhibits a good thermal stability: the pyrolysis temperature is around 550°C, the melting point is ≈ 343°C and the glass transition temperature is ≈ 145°C [15]. This range of temperatures is particularly high for a polymeric material. In addition, it has a good behaviour in corrosive environments, in fact it is insoluble in all common solvents, except for strong acids like 98% sulphuric acid and this is the main reason why it is used in the piping system of airplanes. [3]

In order to expand the performance limits of PEEK, it is quite common to reinforce it with a filler giving rise to a composite material. For example, in aerospace, PEEK is usually reinforced with high-strength carbon fibres in structural or prefabricated components. Composite materials are very common nowadays and they find many applications in all industrial fields. The idea behind is to combine the properties of the two starting materials to produce a new one with enhanced properties. For example, the combination of a polymer with carbon fibre can produce a lightweight material with improved mechanical properties. [29]

It is interesting to learn that Victrex, a company which produces PEEK for aerospace applications, reports an increasing number of metal parts being replaced by PEEK composites because, despite the fact that both materials exhibit similar mechanical performance, the composite is significantly lighter, and this allows savings of 10000 \$ in annual fuel costs. The PEEK composite is lightweight, durable, chemical resistant, strong and flame retardant; all of them important characteristics for plane components. Currently the most common composite of PEEK is 90HMF40. [4]

One common composite in the aeronautical and aerospace industry consists in alternating layers of a polymer matrix and a glass or a carbon fibre mat. The in-plane properties of such multilaminar systems can be easily optimized and it is usually the interlaminar properties that limit the overall mechanical performance. The fibre-matrix interfacial bonding plays here a fundamental role and hence, the interphase appears as a critical point to be optimized. Recent studies have highlighted that the mechanical properties of the interphase between the glass fibres and PEEK in multilaminar systems can be improved by adding carbonaceous nanofillers such as carbon nanotubes to the matrix.

In this master thesis, a multilaminar system of PEEK and carbon fibre mats is investigated and graphene is incorporated to the polymer layer with a two-fold aim. On the one hand, it is expected that graphene enhances the mechanical properties of the polymer layer. On the other hand, the mechanical properties at the fibre-matrix boundary can also change with the incorporation of graphene.

The work is divided into three parts. In the first place, the mechanical characterization of free-standing PEEK films by means of indentation is carried out (hardness and modulus values are obtained) and the relationship with average nanostructural parameters is approached. To clarify such relationship, a range of processing temperatures is used, giving rise to different mechanical properties and nanostructures. In the second step, the influence of graphene on the mechanical properties and nanostructure of PEEK is explored. An analysis of the reinforcing effect of graphene is offered. Finally, the mechanical properties of multilaminar systems of graphene-reinforced PEEK and carbon fibre fabric are investigated, with especial emphasis on the possible appearance of an interphase between the fibres and the polymer-based layer.

2. Materials and methods

2.1 Materials

The Polyaryletheretherketone (PEEK) is a semi-crystalline material, comprising repeating monomers of two ether groups and a ketone group.

Figure 1 represents the PEEK basic unit.

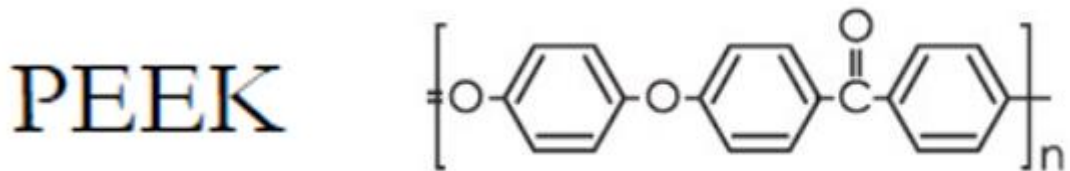


Figure 1. PEEK basic unit [1]

Its good mechanical properties are due to its microstructure and physical properties. Its density is equal to 1,32 g/cm³ and its molecular weight is about 40000 g/mol. PEEK's unit cell is orthorhombic, and the cell parameters are the following: a=7.75 Å b=5.90Å c=9.90Å [3]. The properties depend on the processing history and on the morphology. It can be an amorphous or a semi crystalline material. [20]

Moreover, it is stiffer than many other materials due to the sequence of aromatic rings that compose its structure; for this reason, it shows good mechanical properties at high temperature.

The matrix used was poly(ether ether ketone) in powder form with an average molecular weight of 40,000 g/mol (PEEK 150P) supplied by Victrex, UK. This material has undergone a drying process for one week in order to eliminate all the water presented inside. Phosphorus pentoxide (Panreac) was used for this purpose.

2.1.1 Experiment

The aim of the following experiment is the preparation of amorphous PEEK films using different processing conditions. Figure 2 represents the starting powder of PEEK.

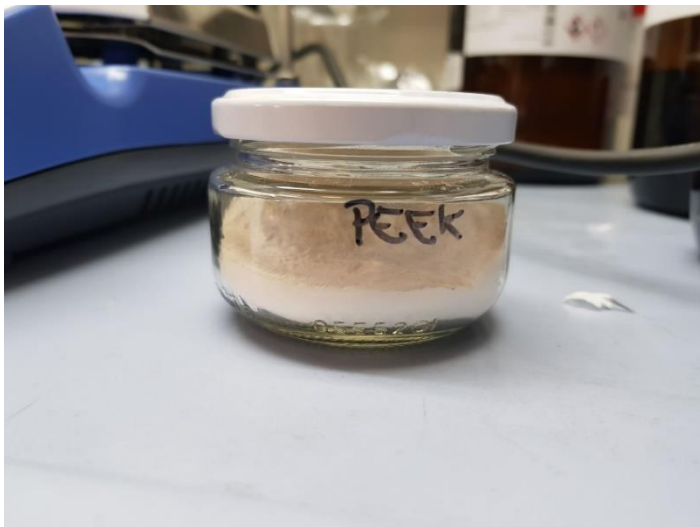


Figure 2. PEEK powder

A small quantity of PEEK powder was deposited with a laboratory spatula between two films of UPILEX, polyimide, previously cleaned with alcohol.

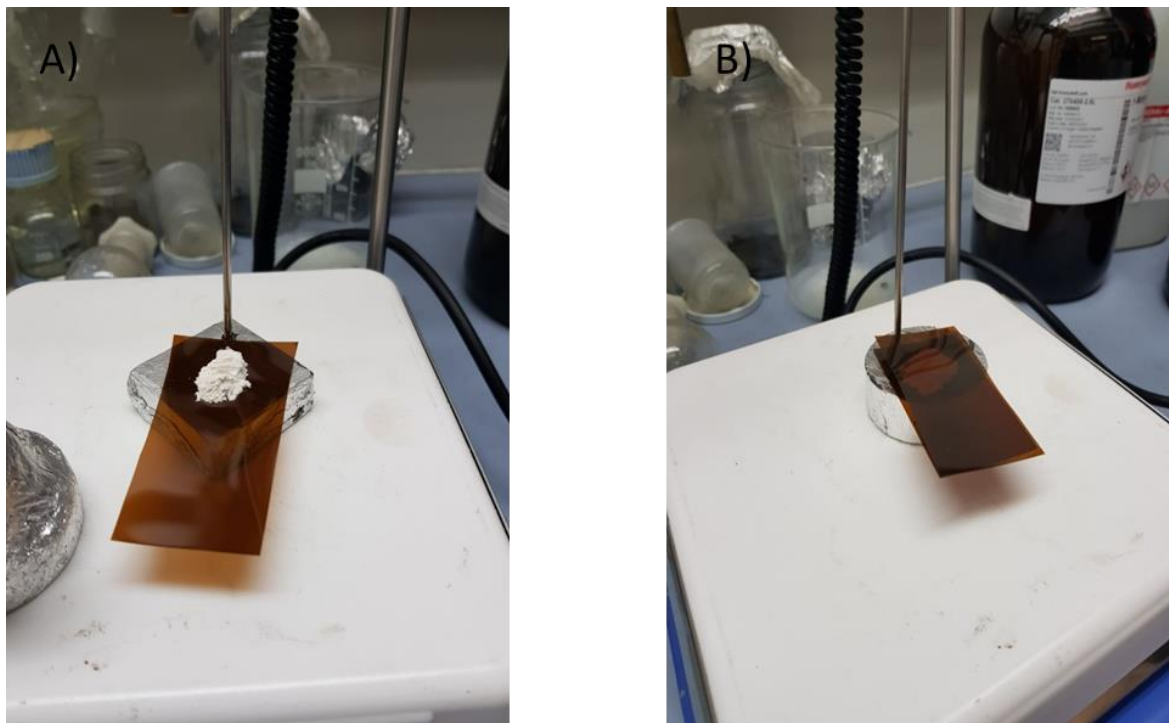


Figure 3. A) PEEK powder with a layer of UPILEX on the heating plate; B) PEEK between two UPILEX's layers before compression

Figures 3A and 3B show the layer of UPILEX lying on the conducting piece.

UPILEX display a high melting temperature and is used to facilitate the removal of the thin layer of amorphous PEEK. In this experiment it is used one weight of 5 Kg as compressor in order to produce thin PEEK layers. These weighs are represented in figure 4.

The heating plate (IKA C-MAG H57) is able to reach a temperature equal to 400°. The real temperature can differ by some degrees from the real one due to energy losses and thermal inertia. The PEEK's melting point takes place around 343°C, however the smaller crystals start to melt at slightly lower temperatures. A thermo-regulator is used to control the temperature. The time of the experiment is at least 5 minutes in order to ensure that all material is melted.



Figure 4. In the left the weights, in the middle the heating machine

After the melting, the PEEK was quenched rapidly: the first time it was put in water- ice, but the result wasn't satisfactory because the cooling rate was not fast enough to inhibit crystallization and produce an amorphous structure.

This experiment was done four times, three times in water-ice, one time in liquid nitrogen. The following samples were obtained:

- **Hy_A1:** quenching in ice and water.
- **Hy_A2:** quenching in ice and water.
- **PEEKN₂:** the cooling process was carried out in liquid nitrogen.
- **Hy_A4:** quenching in ice and water.

The second sample, Hy_A2, seemed amorphous because it was transparent. The third one was put inside liquid nitrogen: the sample obtained was completely crystallized, the aspect was completed opaque. The main explication of this phenomenon is that the cooling rate was too slow possibly due to an inappropriate contact between the liquid nitrogen and the polymer film.

Finally, the fourth sample seemed like the second one.

Figures 5A and 5B show the containers employed for the cooling processes in water-ice and in liquid nitrogen, respectively.

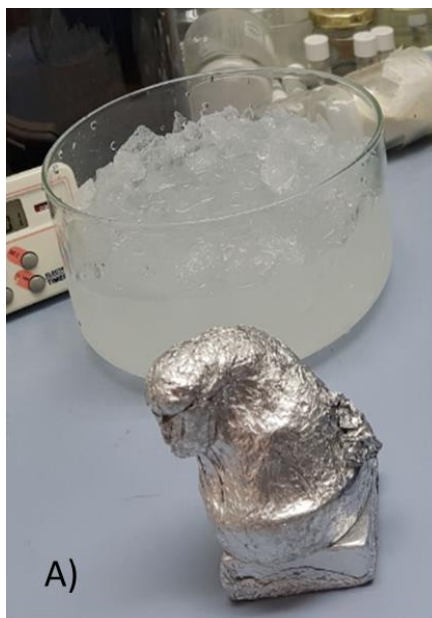


Figure 5. A) Water and ice with weight; B) Liquid Nitrogen

The average thickness of the films was measured and portions of each film were mounted in sample holders for X-ray analysis.

Figure 6A shows a sample holder for X-ray measurements and Figure 6B represents the thickness gauge.



Figure 6. A) Sample holder; B) Thickness gauge

Table 1 shows the average thickness of the samples.

Table 1. First obtained samples

Sample	1 st measurement (µm)	2 nd measurement (µm)	3 rd measurement (µm)	Average thickness (µm)
Hy_A1	288	342	294	308
Hy_A2	331	343	363	344
PEEKN2	275	224	265	254
Hy_A4	335	327	322	328

2.1.2 Calibration

Crystallization from the glassy state (cold crystallization) was carried out using a hot stage (Linkam, THSM 600). Before carrying out the cold crystallization, a calibration of the hot stage was necessary: the temperature indicated does not correspond to the temperature presented on the heating plate due, for example, to thermal inertia. A number of standard materials in powder form and with well-defined melting points were used.

Calibration Samples:

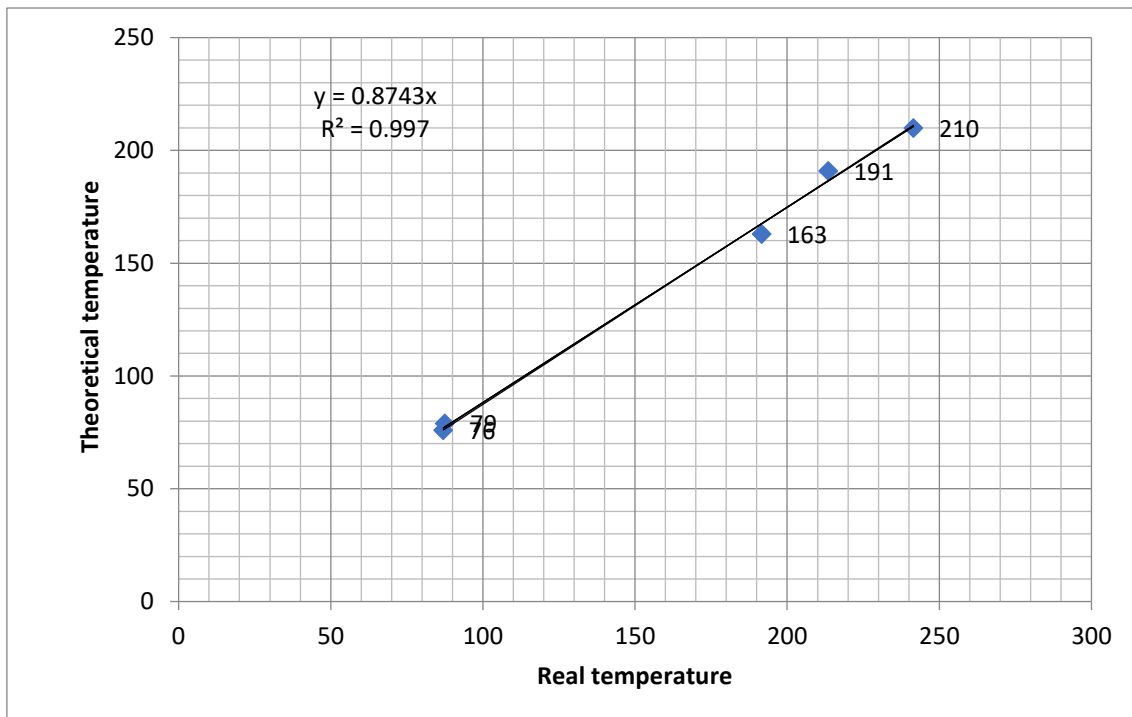
Each calibration sample is placed on the heating stage and heated, first at 10°C/min up to the theoretical melting temperature, and then, at 1°C / minute until the powders melts.

The following table shows the materials used for calibration with the respective temperatures.

Table 2. Powder materials for calibration

Powder material	Theoretical melting temperature (°C)	Real melting temperature (°C)
Salophen	191	225
I-Hexacosanol	79	87.5
Benzanilid	163	191.6
Tetracosanol	76	87

Graphic 1 shows the calibration curve obtained by the correlation between the theoretical and the real temperature.



Graphic 1. Temperature Calibration

With this calibration procedure, one is able to set the temperature in the Linkam in order to carry out the experiment.

2.1.3 Cold Crystallization

Starting from the amorphous samples, a number of semicrystalline samples were prepared. The cold crystallization technique was used: the glassy sample is heated at a temperature above the glass transition temperature, T_g , for a period of time long enough to allow crystallization.

Table 3 represents the different samples, the crystallization temperatures and the crystallization times.

Table 3. Nomenclature used for PEEK samples cold crystallized at different temperatures. A Linkam hot stage was used and the temperature was raised at 10°C/min from room temperature.

Sample	Theoretical temperature (°C)	Real Temperature(°C)	Exposure Time (min)
PEEK166.1h	166	190	60
PEEK150.1h	150	171	60
PEEK156.12h	156	178	720

PEEK175.1h	175	20	60
PEEK220.1h	220	251	60
PEEK166.12h	166	190	720
PEEK166.1hNEW	166	190	60
PEEK240.1h	240	274	60
PEEK156.1h	156	178	60
PEEK185.1h	185	212	60
PEEK160.1h	160	183	60
PEEK240.1hN	240	274	60
PEEK145.1h	145	166	60

Figure 7 shows the Linkam hot stage used for the cold crystallization. The system includes a computer, that sets the temperature rates and the time, and two sample holders.



Figure 7. Linkam

The main challenge is to obtain samples without local molecular orientations because it is well known that preferential orientations could influence the mechanical properties and it is convenient not to have this additional factor in our data analysis. However, we firstly obtained

samples with preferential orientations. Hence, a procedure was developed to avoid such orientations, as will be explained below.

2.1.4 Preparation of samples

The evaluation of the mechanical properties was carried out using a nanoindenters G200 (Keysight Tech., USA). For this process, the preparation of the sample surface is critical. The main objective is to reduce as much as possible the surface roughness of the samples, through different polishing processes. [10] [12]

Firstly, PEEK samples are placed vertically together in a plastic holder, shown in figure 8.

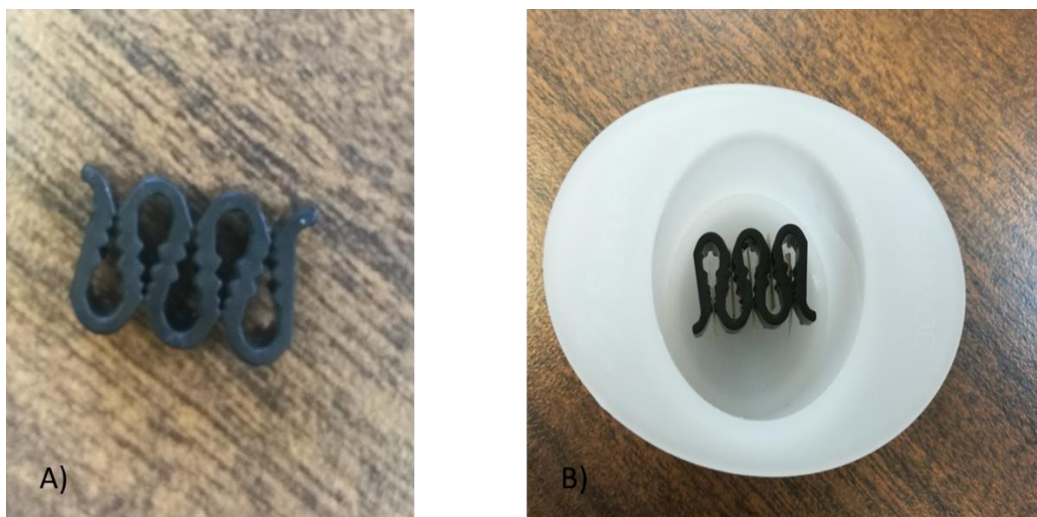


Figure 8. A) Plastic holder clip; B) Plastic holder clip with mold

Subsequently, the sample preparation is started: the plastic holder is embedded in a mixture of resin and hardener until it stiffens. The hardener is slowly added to the resin. A wooden spatula is used to mix them very carefully in order to not generate bubbles. Finally, it is poured into the plastic mold with a diameter of 30 mm and left to dry for at least a day. [11]

Subsequently, it is necessary to cut the sample in order to expose the PEEK on the surface using a microtome illustrated in figure 9. This instrument is set up in such a way to continuously cut 3 or 4 microns of material in each cycle. To assess, if the PEEK samples are on the surface, small cracks will be observed on the 3/4-micron lamina of the epoxy resin.

Before cutting the sample, the head of the microtome was adjusted to place the sample in a perfect vertical position. In addition, the cutting speed as well as the layer thickness (3-4 micron) can be selected.



Figure 9. Microtome

Finally, in order to minimize the roughness, a polishing process was accomplished. In general, four polishing steps were carried out using different silicon carbide papers with progressive final grade. The machine is an automatic grinder-polisher (Buehler, USA) with a polishing speed of 150 rpm and a downward force of 50N [11], represented in the following image.



Figure 10. Polishing Machine

The first step involves the use of a silicon carbide paper of P1200, the force applied is about 50N and the speed rotation is 150 cycle/min. This process runs for 4 minutes. The second step involves a silicon carbide paper of P1500 during 4.5 minutes.

The third step lasts 5 minutes and further decreases the roughness using a silicon carbide paper of P2500. Finally, a paper of P4000 for 5 minutes is used. The whole process is performed with

water to reduce the temperature that can be generated and to reduce the friction: the water is used as a lubricant. To conclude the polishing step, a microcloth (Buehler, USA) saturated with alumina solution of 0.6 mm particle size, is used for surface finish. [11].

The mechanical properties of the samples are analyzed and studied by means of a nanoindenter. This equipment employs a nanometer-sized tip: the smaller the tip, the lower should the roughness be to achieve meaningful data.

Figure 11 shows selected samples after the polishing procedure. Samples are placed on the platform of the G200 nanoindenter, as explained later in the text.



Figure 11. Final samples

2.1.5 Composite Materials

As already mentioned in the introduction, the main goal of this work is to understand how graphene affects the microstructure and the mechanical properties of PEEK and how much it helps to achieve a better adhesion between the carbon fibers and the PEEK matrix in order to decrease the interlaminar fracture.

The composites materials used are mounted in the plastic clip shown in figure 12. The samples used in the present study are the following (starting from the left-hand side):

- The first sample is a multilaminar composite of PEEK with carbon fiber, named “PEEK+CF1”. It is composed by 10 layers of PEEK and 9 layers of carbon fiber. Its composition is 71.5% in weight of carbon fiber and 28.5% in weight of polymer.
- The third one is an amorphous PEEK used as a reference.
- The fourth one is a PEEK-based nanocomposite with 5 wt.% of graphene and 5 wt.% of sulfonated PEEK, named “5GsPEEK”, represented in picture 13. The sulfonated PEEK is used to help effectively dispersing graphene in the matrix.
- The last one is a multilaminar composite containing 10 layers of reinforced PEEK and 9 layers of carbon fibre fabric, named “PEEK+CF3Gs”. It is composed by 69% in weight of carbon fiber and 31% of nanocomposite. The reinforced PEEK includes 5 wt.% of graphene and 5

wt.% of sulfonated PEEK, i.e., it is exactly the same nanocomposite as the one described in the fourth place.

These compositions are determined by thermogravimetric analysis in a nitrogen atmosphere.



Figure 12. Embedded PEEK-based samples



Figure 13. PEEKGs sample

2.2 Methods

2.2.1 X-ray analysis, material characterization

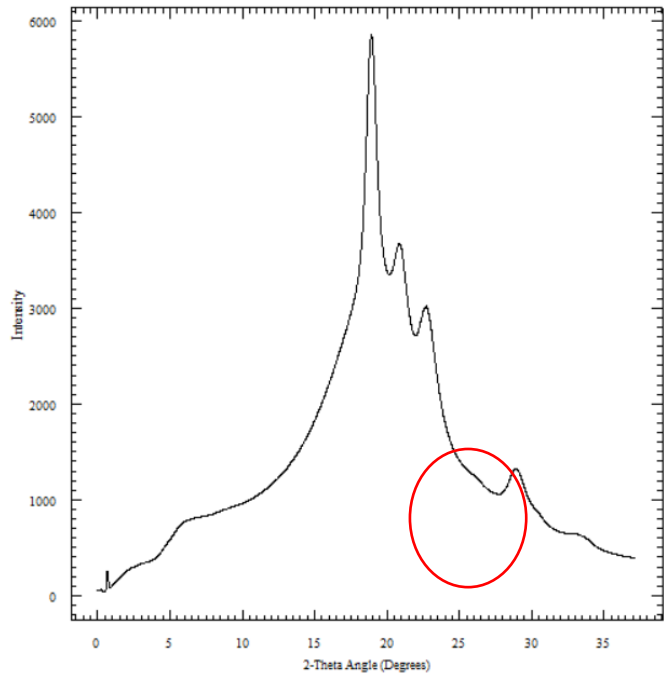
The X-rays are a form of electromagnetic radiation as visible light or infrared, but they have a wavelength around 1 Angstrom. This kind of radiation is used in crystallography, field that studies the nanostructure of materials, because the wavelength is close to the distance between atoms or molecules. In this work, X-ray diffraction is used to analyze amorphous and crystalline materials and in the latter case, a quantitative evaluation of the amount and quality of the crystal phase is given. Generally, X-rays' frequency is about 3 million THz and the energy about 12,4 keV. The source of X-ray diffraction can be diverse including high voltage generators (50.000 volts) and incandescent filaments usually of tungsten. [21] [8]

2.2.2 Process

In an X-Ray tube, electrons at the cathode are accelerated and X-rays are generated by their collision with the anode. These high energy electrons generate two types of radiations. The first one is called Bremsstrahlung: an electron goes very close to the nucleus target and it changes the path for the electromagnetic interaction, it losses a lot of energy and generates a photon. The second radiation is called X-rays: an electron with really high energy is able to displace an electron very closed to the nucleus target. The hole formed by this displacement is filled by an electron set in a higher energy levels. The difference between the higher energy level and the lower one, set the energy of the monoenergetic photon, called X-Rays. [21]

The interaction between the X-Rays and the material gives a physical phenomenon called diffraction. In the present experiments, wide angle X-ray scattering (WAXS) is employed. WAXS refers to diffraction angles, 2θ , greater than $\approx 1^\circ$. A Micro Star rotating anode generator (Bruker) operating at 100mA and 50kV is used (see Figure 14). The diffraction patterns are recorded using a Mar345 image plate. The resolution is equal to 3450x3450 pixels with 100 $\mu\text{m}/\text{pixel}$. The wavelength is $\lambda=0.1542 \text{ nm}$ and the distance between the sample and the detector is 220 mm. The analysis of the diffraction patterns is carried out using the FIT2D software, in particular the program allows azimuthal integration and can provide profiles of diffracted intensity as a function of diffraction angle 2θ . [11]

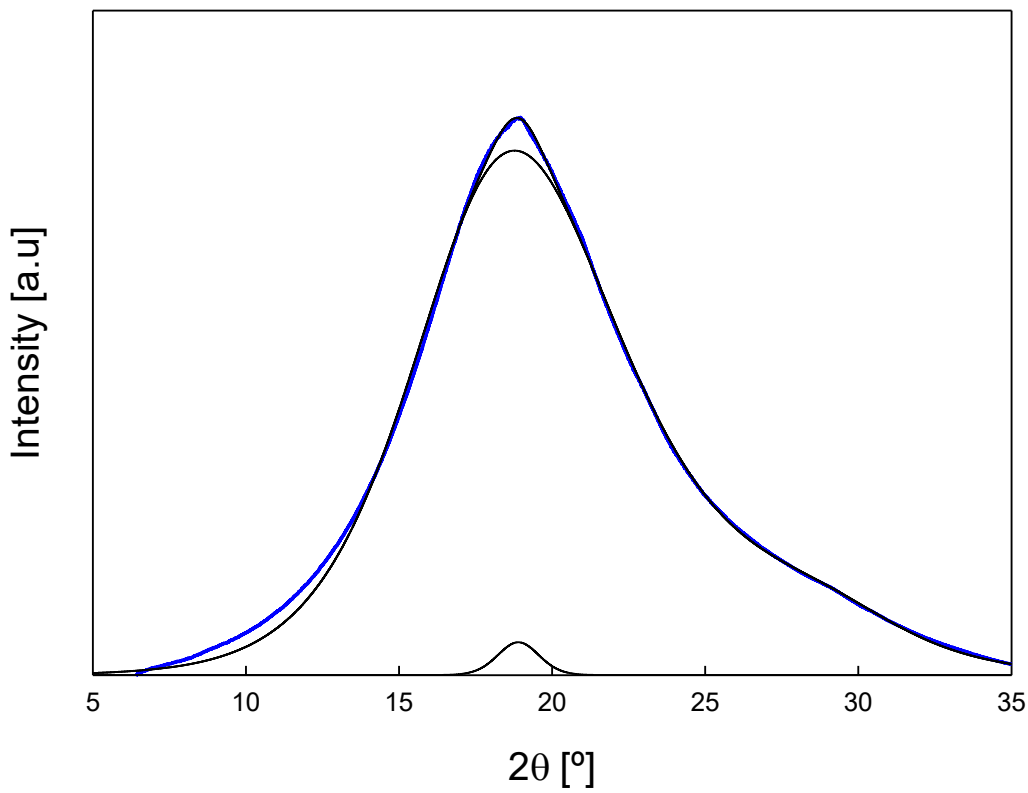
To correct for background, a numerical factor of ≈ 0.96 is used. This allows removing the scatter of the air and other instrumental effects (see plot 1).



Plot 1. 1D integration without removing the background

Furthermore, Peakfit v4.12 software is used to fit the 1D intensity profile to two different type of functions: Pearson VII for the crystalline peaks and Asym Dbt for the amorphous halo. [11]

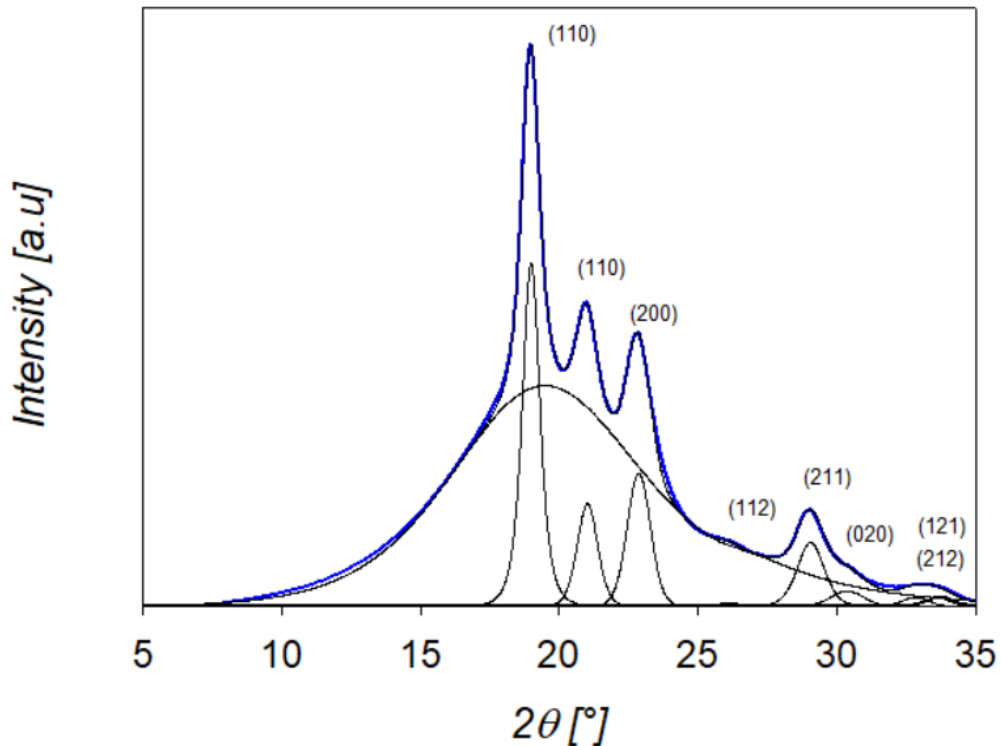
The 1D profiles are used to evaluate the crystallinity of each material. As an example, Plot 2 shows the deconvolution of HyA2. It is found that the intensity diffraction curve can be separated into one asymmetrical curve representing the amorphous halo and one Pearson function accounting for one crystalline peak (due to the low levels of crystallinity only one maximum can be found).



Plot 2. Deconvolution Hy_A2

Analysis of the data of Plot 2 yields $\approx 1\%$ crystallinity. The small peak at $2\theta = 18.78^\circ$ corresponds to the plane (110). Plot 3 illustrates, as an example, the intensity profile of one semicrystalline PEEK sample. The most intense maxima of the crystalline structure of PEEK can be identified on this plot and are the following [2][28][20]:

- (110) diffract at 18.78°
- (111) diffract at 20.74°
- (200) diffract at 22.79°
- (112) diffract at 26.01° , very difficult to see.
- (211) diffract at 28.82°
- (020) diffract at 32°



Plot 3. PEEK' planes

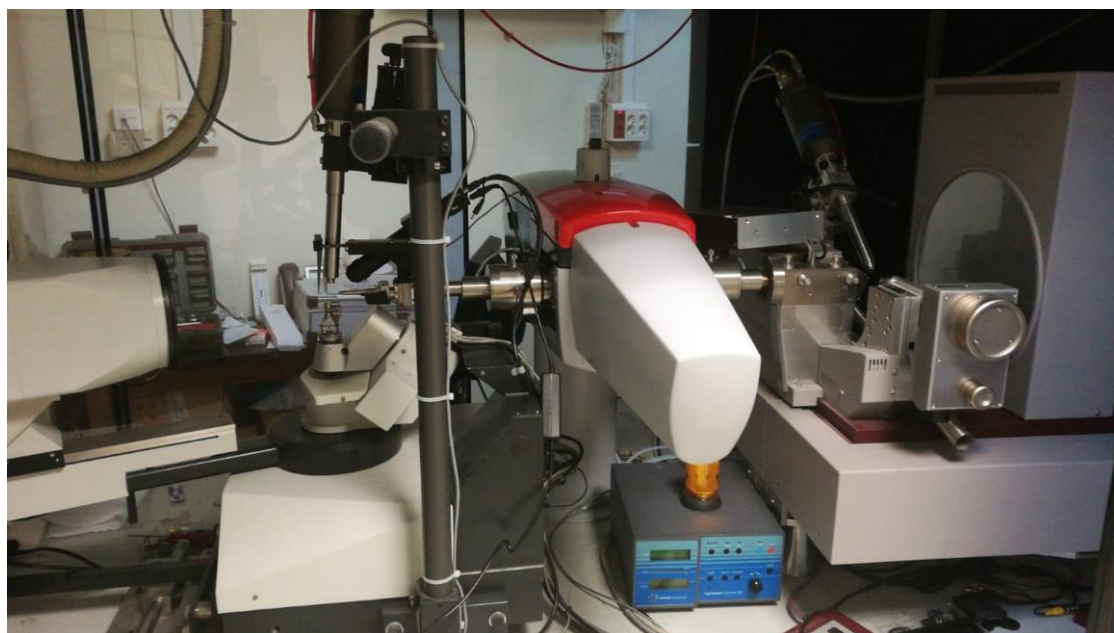


Figure 14. Micro Star rotating anode generator and detector

Moreover, the crystallization speed reaches a maximum value between 200°C and 280°C , outside this range the crystallization kinetics drastically falls off [2], as we can see in the following graph.

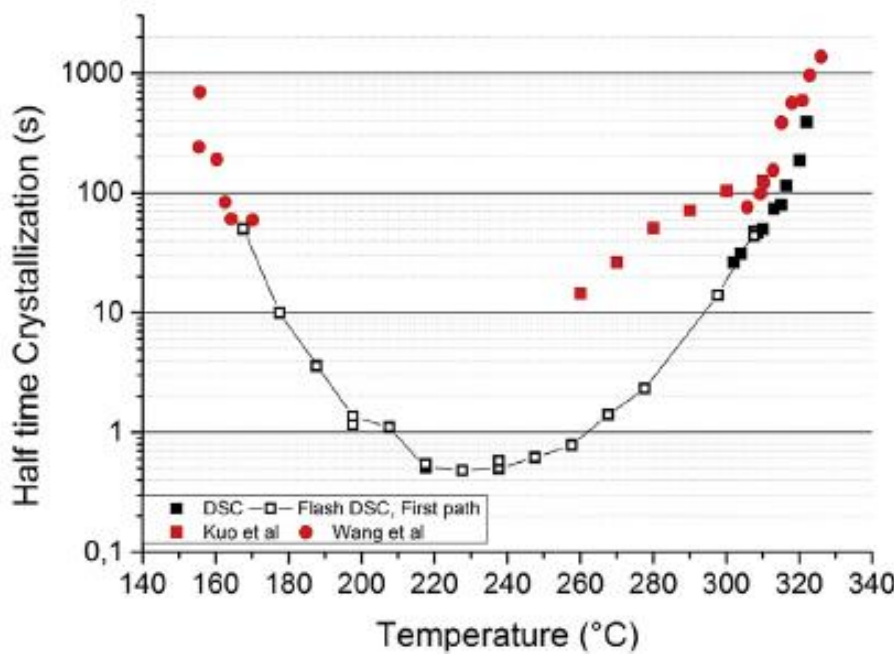


Figure 15. Crystallization kinetics [15]

The half time crystallization, showed in the graph, is defined as the time at which the degree of crystallinity is the half:

$$\alpha(t_{0.5}) = 0.5 \quad (1)$$

The curve is a parabola and it shows that the lowest crystallization half-time is between 230°C and 240°C. Over 280°C and under 200°C, the crystallization half-time increases very quickly since crystallization is increasingly controlled either by diffusion at low temperatures or by nucleation at high temperatures. [15]

2.2.1.1 Lateral crystal size determination

The dimension of the grain size is an important parameter since the mechanical properties depend on the crystal size. The lateral crystal size (D_{hkl}) is calculated by the Scherrer's equation:

$$D_{hkl} = \frac{\lambda}{\beta \cos(\theta)} \quad (2)$$

Where:

- D_{hkl} : crystal dimension
- β : FWHM (full width at half maximum)

On the other hand, it is well accepted that the hardness is additive property of the crystalline and the amorphous regions:

$$H = H_c X_c + H_a (1 - X_c) \quad (2.1)$$

Where:

- H_c : average hardness of the crystals
- X_c : crystallinity degree
- H_a : average hardness of the amorphous regions

The average hardness of the crystal is related to the crystal size following:

$$H_c = \frac{H_o^\infty}{1 + \frac{b}{l_c}} \quad (2.2)$$

Where:

- H_o^∞ : the hardness of the infinitely large crystal
- b : Depends on the surface energy
- l_c : crystal thickness

With the equation number 2.2, it is clear that if the dimensions of the crystal are big, the average hardness increases.

The crystallinity degree is calculated using WAXS data, from the ratio between the crystalline area and the total area.

$$X_c = \frac{A_c}{A_t} \quad (2.3)$$

2.2.2 Mechanical properties from nanoindentation: correlation with nanostructure

2.2.2.1 Introduction to nanoindentation

An indenter is a tool with controlled geometry and known mechanical properties that is put in contact with a sample. Indentation techniques are based on the local deformation produced on the surface of a sample upon application of a load. The size of the indentation depth determines whether macro-, micro- or nano-indentation is employed. Additionally, important differences are found between the modes of operation of each technique. [9] [12]

In macro- (or simply, indentation) and micro-indentation, the dimension of the footprint is determined by optical means and the methodology is quite simple and robust. In the case of microindentation, an optical microscope is required to measure the size of the residual indent.

Instrumented indentation testing (IIT), or nanoindentation, or depth-sensing indentation, is not based on optical instrumentation but on the monitoring of the continuous deformation of a sample as the load is incremented. The size of the indentations can vary from only a few nanometers up to a few micrometres. Although the terminology “nanoindentation” should strictly apply to indentation depths in the nanometer scale, it is commonly used for tests involving penetrations in the micrometer scale, as long as an instrumented indentation tester is employed. [12]

Nanointentation was developed in the late eighties to study the mechanical properties of thin films and coatings, not accessible by optical means due to the size of the residual depth. In addition, nanoindentation can be used to map the mechanical properties at low spatial resolution. A typical depth-sensing test involves a loading and an unloading cycle, using a load cell and a displacement sensor that varies according to the type of instrument. One additional advantage of nanoindentation is that it can provide information on Hardness, H , which can be defined as the mechanical resistance to plastic deformation, and Elastic modulus, E , related to the stiffness of the material. In traditional indentation testing, based on optical measurement, only Hardness values are usually reported.

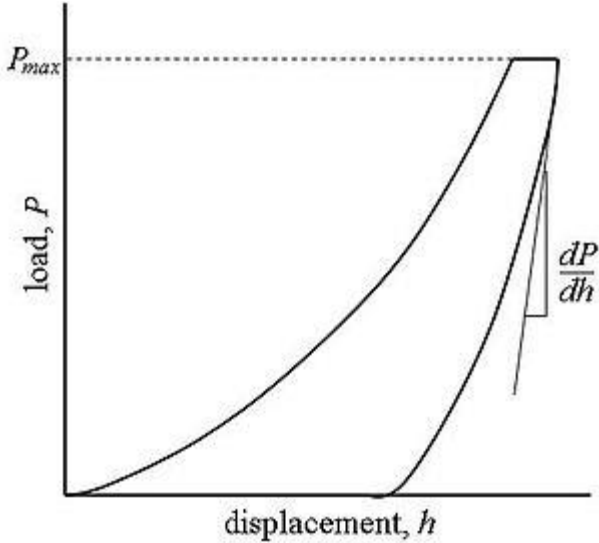
In IIT, a number of assumptions need to be considered in order to derive the H and E values from the analysis of the load-depth data. Such assumptions seem quite reasonable for metals and ceramics, however, their application to polymer materials, with time-dependent properties, is quite controversial, as will be mentioned below.

Hardness and the elastic modulus are intimately related to the chemical elements along the polymer chain and to the final arrangement to conform the material nanostructure. Hence, changes in the nanostructure should be readily detected by indentation. For instance, the degree of crystallinity and the lamellar thickness are parameters that can describe a polymer nanostructure and that are expected to influence the mechanical properties.

2.2.2.2 Oliver-Pharr method

Graphic 2 illustrates, as an example, a load-hold-unloading curve obtained using a depth-sensing indentation system. This curve is characterized by a loading cycle where elastic-plastic deformations take place and an unloading curve where elastic deformations recover. Analysis of the load-displacement curves is often based on the work by Oliver and Pharr. This method

is based on the assumption that there is a pure elastic contact at the beginning of the unloading and suggests a procedure to calculate the contact stiffness S and the projected area of contact between indenter and sample, A , at maximum load. [9] [12] [14]



Graphic 2. Load vs Displacement [23]

The slope of the unloading curve at maximum load and displacement defines S . The contact depth, h_c , which is used to calculate A , is related to the extrapolation of the tangent at $P = 0$, as indicated below. The contact area depends on the geometry of the indenter and for a Berkovich tip, $A = 24.5h_c^2$. [12] [13]

The Oliver-Pharr method assumes:

- The material is homogeneous and isotropic
- Fully elastic recovery at the beginning of the discharge

The reduced modulus E_r is related to S and A through:

$$E_r = \frac{\sqrt{\pi} \cdot S}{2 \cdot \sqrt{A} \beta} \quad (3.1)$$

where β is a constant that for a Berkovich tip is equal to 1.034.

To determine the contact depth from the experimental data, the following formula can be used:

$$h_c = h_{max} - h_s \quad (3.2)$$

Where h_{max} is measured experimentally and h_s , the elastic displacement of the surface, is equal to:

$$h_s = \frac{P_{max} \cdot \epsilon}{S} \quad (3.3)$$

Where ε is a geometric constant that depends on the geometry of the tip: in our case ε is equal to 0.75.

Finally, the modulus can be calculated, provided Poisson's ratio (ν) and the indenter properties are known:

$$\frac{1}{E_r} = \frac{1-\nu_s}{E} + \frac{1-\nu_i}{E_i} \quad (3.4)$$

where the subscript "s" stands for sample and "i" for indenter. [14]

Figure 16 illustrates schematically the indentation process at maximum load and displacement.

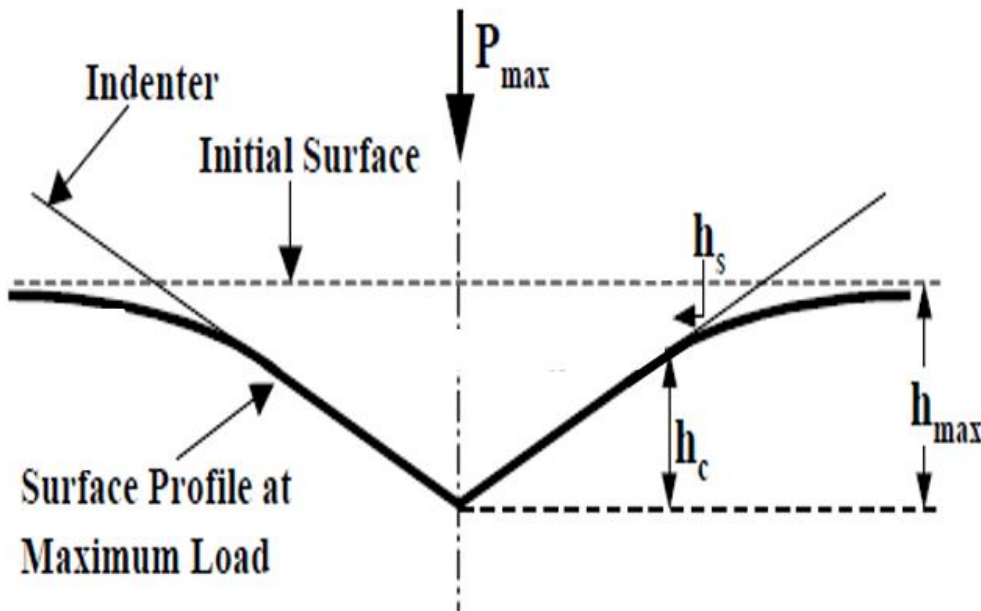


Figure 16. Indentation geometry at maximum load for a conical indenter [14]

However, in the case of polymers, it is quite common that Oliver-Pharr's method cannot be applied because a "nose" appears at the beginning of the unloading cycle. This particular shape is the consequence of the time-dependent properties of polymers that creep under application of a constant load. A number of approaches have been suggested to overcome this problem. For example, some researchers use long holding times and high unloading rates to dissipate creep. However, values of S unaffected by testing conditions can never be guaranteed. Another approach is to use the continuous stiffness measurement. [10] [12]

2.2.2.3 Application to polymers: Continuous Stiffness Measurement (CSM)

Continuous stiffness measurements (CSM) is based on the overlapping of a small sinusoidal force to the primary load signal and analyzes the phase lag between applied force and displacement of the machine-material system (see Figure 17). This method offers the possibility

to calculate the hardness and the elastic modulus as a function of the depth at every stage of the loading cycle.

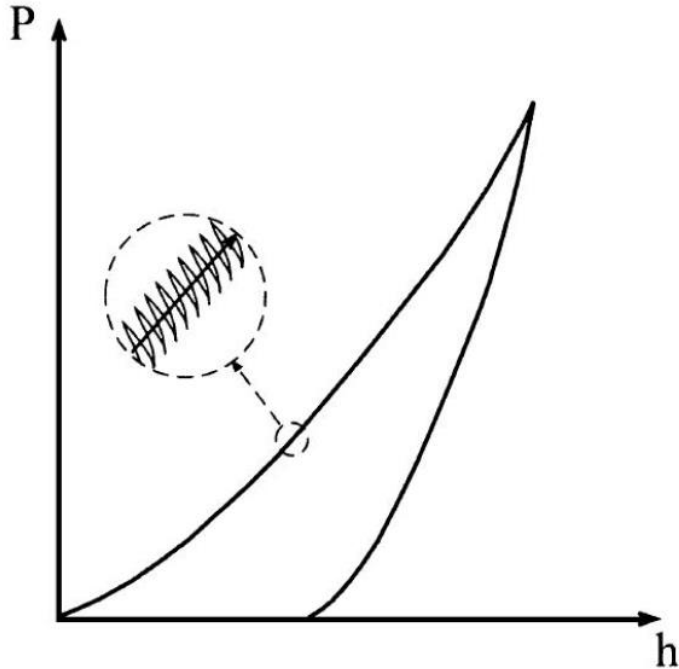


Figure 17. CSM technique [16]

The movement of the indenter is constrained to vertical translation, in such a way that can be modelled as an elementary harmonic oscillator. The sinusoidal force imposed is equal to:

$$F(t) = F_0 e^{i\omega t} \quad (4.0)$$

The vertical displacement is equal to:

$$z(t) = z_0 e^{i(\omega t - \phi)} \quad (4.1)$$

In other words, the displacement oscillates at the same frequency as the imposed force (ω), but it is offset by an angle ϕ . [9]

In CMS, the operator imposes the force and the frequency ω , whereas the oscillation amplitude and the phase lag are recorded experimentally. [9]

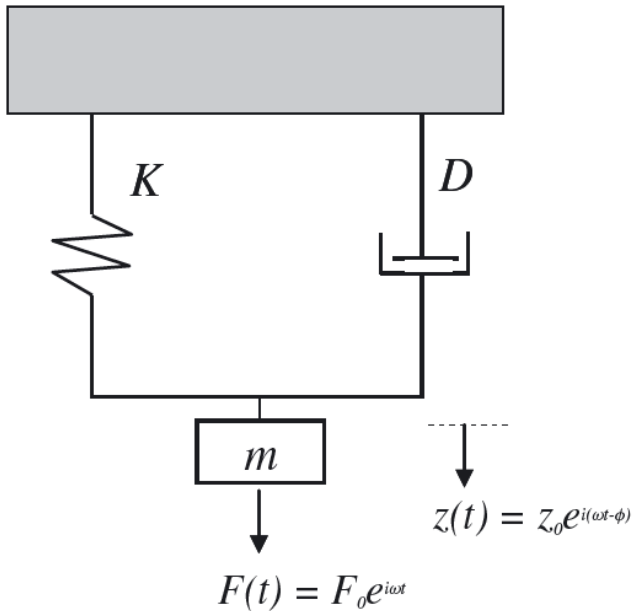


Figure 18. Simple harmonic oscillator

Figure 18 illustrates the mechanical model for a simple-harmonic oscillator. By applying this model, first to the indenter alone, and afterwards, to the indenter-sample contact, one can arrive to:

$$S = \left[\frac{1}{\frac{F_0}{z_0} \cos \phi - (K_i - m\omega^2)} - \frac{1}{K_f} \right]^{-1} \quad (4.2)$$

K_i, K_f are calibration constants, and m is the indenter mass (provided by the manufacturer).

Using equation (3.2), one can determine S as a function of displacement over the entire loading cycle.

For a viscoelastic material, such as polymers, the complex modulus is $E^* = E' + i E''$, where $E'' = E \sin \phi$ and $E' = E \cos \phi$ represent the loss and storage modulus, respectively. [12] Using elastic-viscoelastic correspondence, equations 4.1 and 4.4 can be used to derive the storage modulus E' .

2.2.2.4 The indenter

The indenters used in these tests differ from each other not only from the shape but also from the material that make them up. The main shapes used are tetrahedral, spherical or pyramidal, whereas the main materials used are tungsten carbide, steal and diamond. The types of materials used and the types of shapes, that form the indenter, can favor either the elastic or the plastic behavior. To study the properties of polymeric materials it is customary to use pyramid-shaped diamond indenters to limit the elastic behavior and increase the plastic one, especially in the traditional technique enhancing the plastic deformation makes hardness values more

meaningful. [12] In this work a G200 Berkovich nanoindentator was used, which has three-sided pyramidal tip. The force is applied through a magnetic winding, varying the intensity of the circulating current. A capacitive sensor consisting of three plates instead provides the displacement measurement: one connected to the indenter and the other two fixed. The Berkovic indenter is used in nano-scale indentation studies because it has the advantages that the edges of the pyramidal shape are easily constructed to meet at a single point. The face angle is in general set at 65,27°. The dimension of the tip is in the order of 50-100nm. [12] [14]

During indentation it is better to use the pyramidal tip than a sphere tip because the first one produces less concentration of stresses and because a pyramidal geometry limits the elasticity and magnifies plastic deformation making the values of the hardness more significant.

The hardness can be calculated as the ratio between the applied load P and the contact area between the sample and the indenter, assuming the irreversible plastic deformation and that the time dependency is analyzed by changing the loading time:

$$H = \frac{P_{max}}{A_c} \quad (5)$$

The final fraction of the depth recovery is intimately related to the material yield stress (or hardness) to modulus ratio that in turn, changes with the chemical architecture along the chain, the molecular weight, the degree of crystallinity, etc.

However, before analyzing the samples, it was necessary the tip calibration in order to do a good experiment. The tip calibration is carried out in a series of indentations on fused silica ($E=72$ GPa) because E and H are independent of the indentation size. [12] In addition, in our experiment, when the force increases almost instantly of 100 N/m we consider that the tip detects the surface of the sample. The force has been set at 100 N / m because the indenter, measuring at nanometric scales, is very sensitive to possible vibrations developed in the neighboring environment like a person walking or closing a door. [12]

2.2.2.5 Correlation of hardness and Young modulus with nanostructure

The hardness of a polymer material is controlled, in the first place, by the chemical composition of the repeat unit. Indeed, higher values of hardness are found when the stiffness of the polymer chain increases. For example, when a polymer is composed by aromatic rings, the mechanical properties tend to be higher than those with a high flexibility along the chain. In addition, hardness depends on other structural factors such as the packing of the crystalline structure or the amount of crystalline phase. Every polymeric material has a range of hardness values depending on the fraction of crystalline phase. For instance, figure 19 shows hardness values obtained by optical measurement for a number of polymers. One can see that there is an interval of H values for PEEK from 120 MPa to 600 MPa based on the amount of crystalline phase. The shaded part of the bars corresponds to values measured experimentally while the unshaded part corresponds to extrapolated values. Hence, the minimum H value measured experimentally for PEEK ($H = 120$ MPa) is associated to the glassy material while the maximum one ($H = 300$ MPa) corresponds to a degree of crystallinity of $\approx 40\%$. In this representation, PEEK shows the

highest hardness value of all materials because it has strong intermolecular forces holding the molecular chains within the crystals. [12]

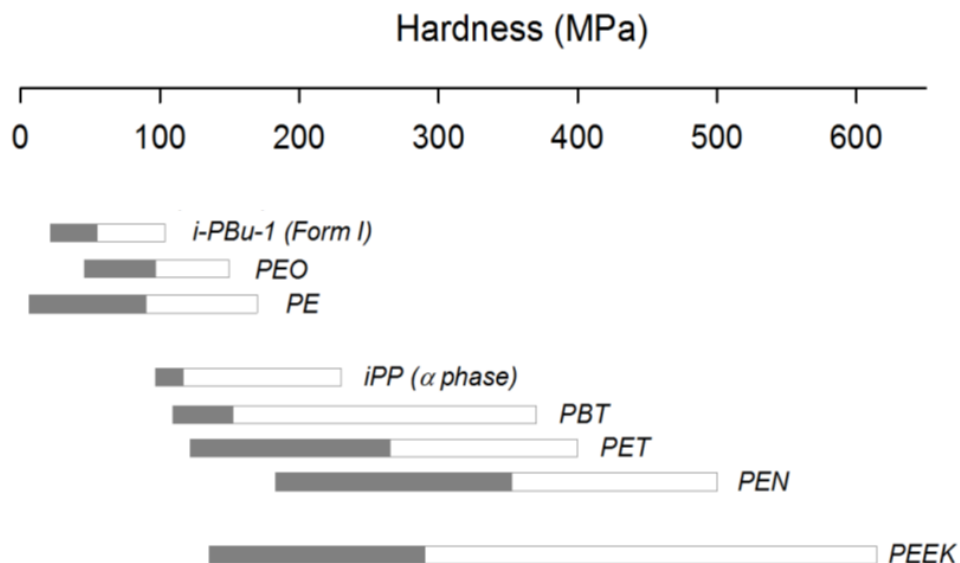


Figure 19. Hardness, determined by optical method, for a number of polymers [12]

A linear extrapolation of the results yields a maximum theoretical H value for fully crystalline PEEK of 730-750 MPa, as can be found in figure 20. It is noteworthy that the range of hardness values obtained from nanoindentation is shifted upwards with respect to those reported by optical means. This difference is due probably to the two different kinds of measurement, one based on the optical measurement after load release, and the other (CSM) under load and based on depth-sensing instrumentation.

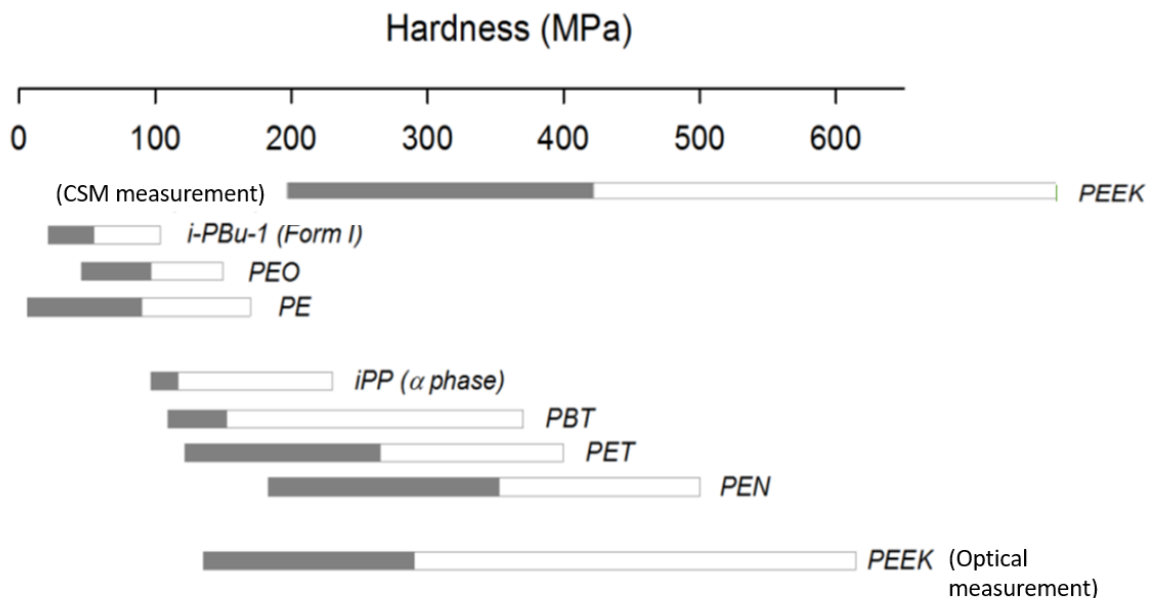


Figure 20. Comparison of the mechanical properties obtained with the optical method and those obtained with CS

3. Results and discussion

3.1 PEEK

3.1.1 Nanostructure by means of the X-ray diffraction

From the cold crystallization process, several samples with different crystallinity degrees were obtained. Diffraction patterns of such samples are different depending on the crystallinity degree. Figure 21 shows the diffraction pattern of the first sample quenched in ice.

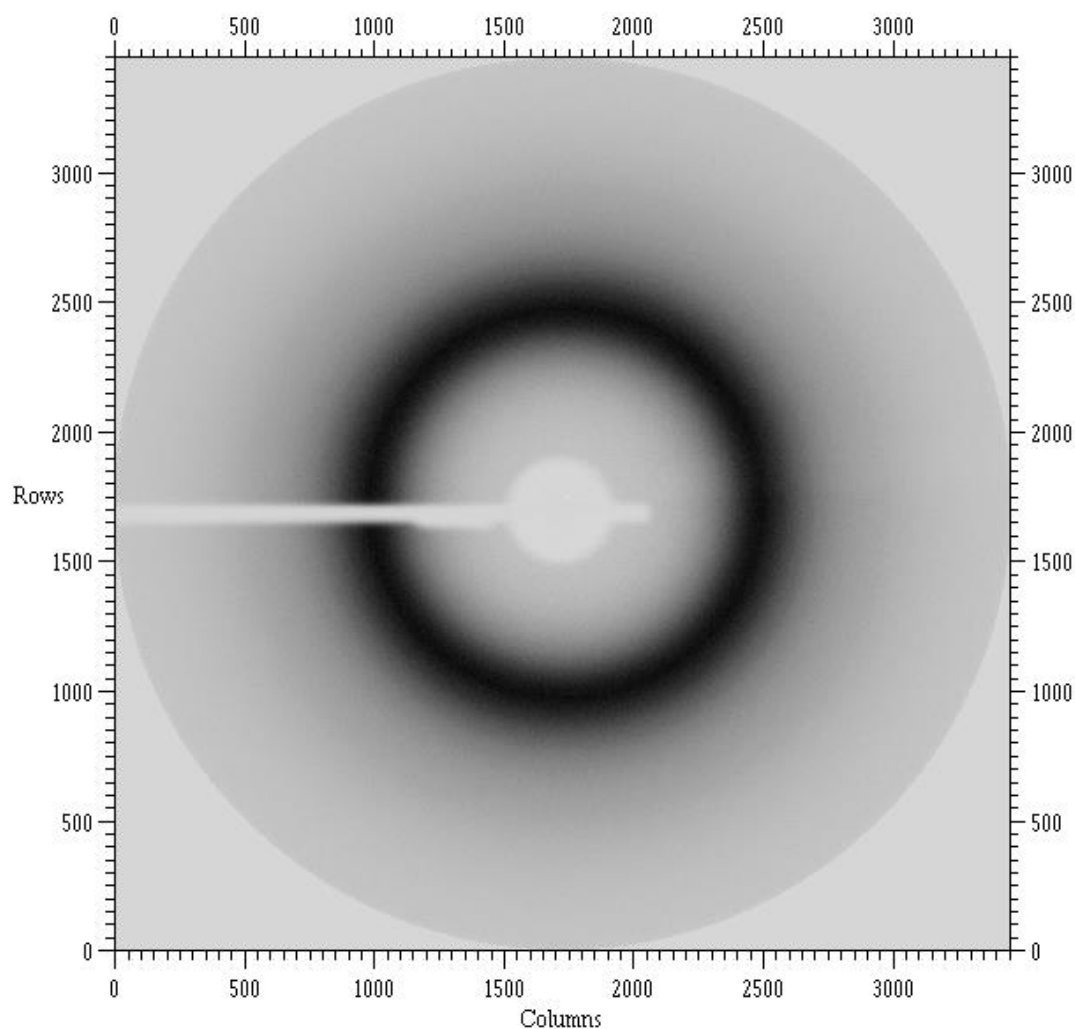


Figure 21. Hy_A2 diffraction pattern

From this picture, at first sight, an amorphous halo characteristic of a non-crystalline material can be distinguished. No significant crystalline peaks can be found. The white part mark in the

central part of the pattern corresponds to the beam stop, which is made out of lead to absorb the incident radiation and protect the detector.

On the other hand, Figure 22 shows a semicrystalline PEEK material with the respective crystalline planes. [29]

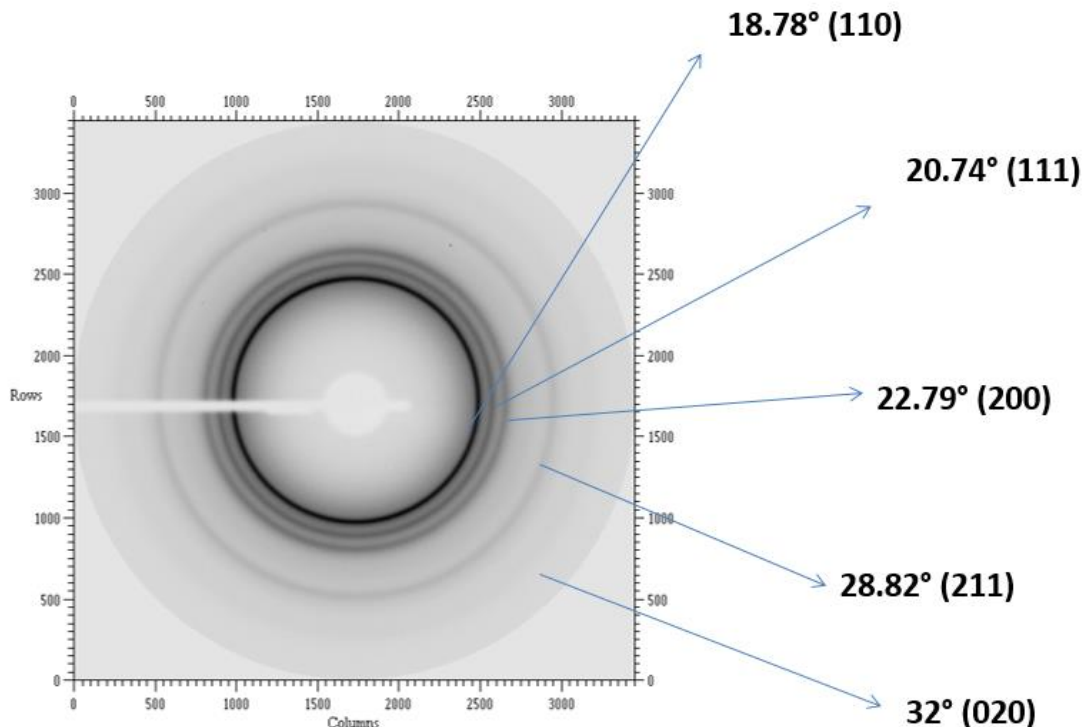


Figure 22. Semi-crystalline material and respective planes

Figure 23 shows the intensity profile of the PEEK sample cold crystallized for one hour at 145 °C. The degree of crystallinity is equal to 4%. Figure 24 shows similar results for a sample with an intermediate degree of crystallinity (17-18%). In this case, a number of crystalline peaks can be distinguished. Finally, Figure 25 shows results for the PEEK sample with the highest degree of crystallinity (26%). In this latter case, the peaks are clearly narrower.

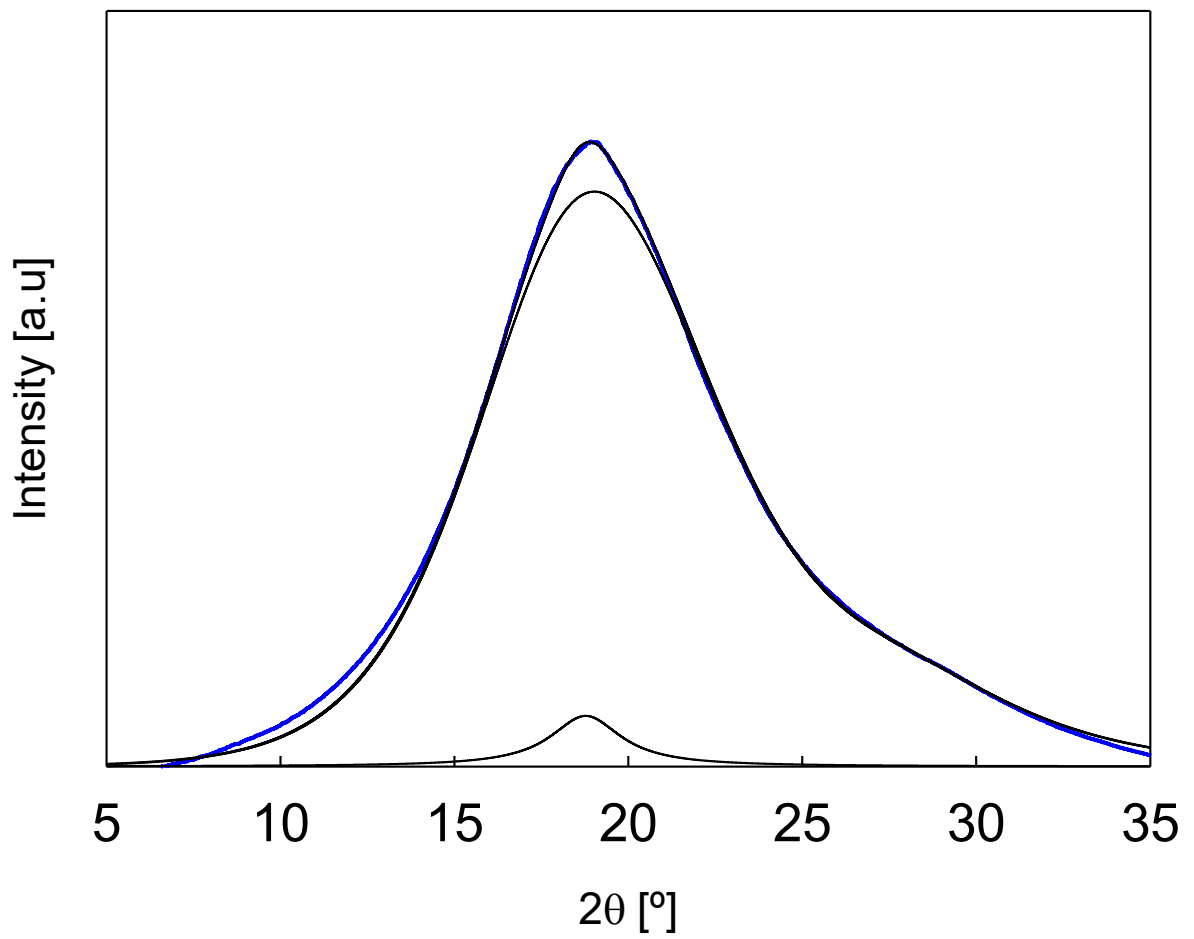


Figure 23. Sigmaplott deconvolution of PEEK145.1h

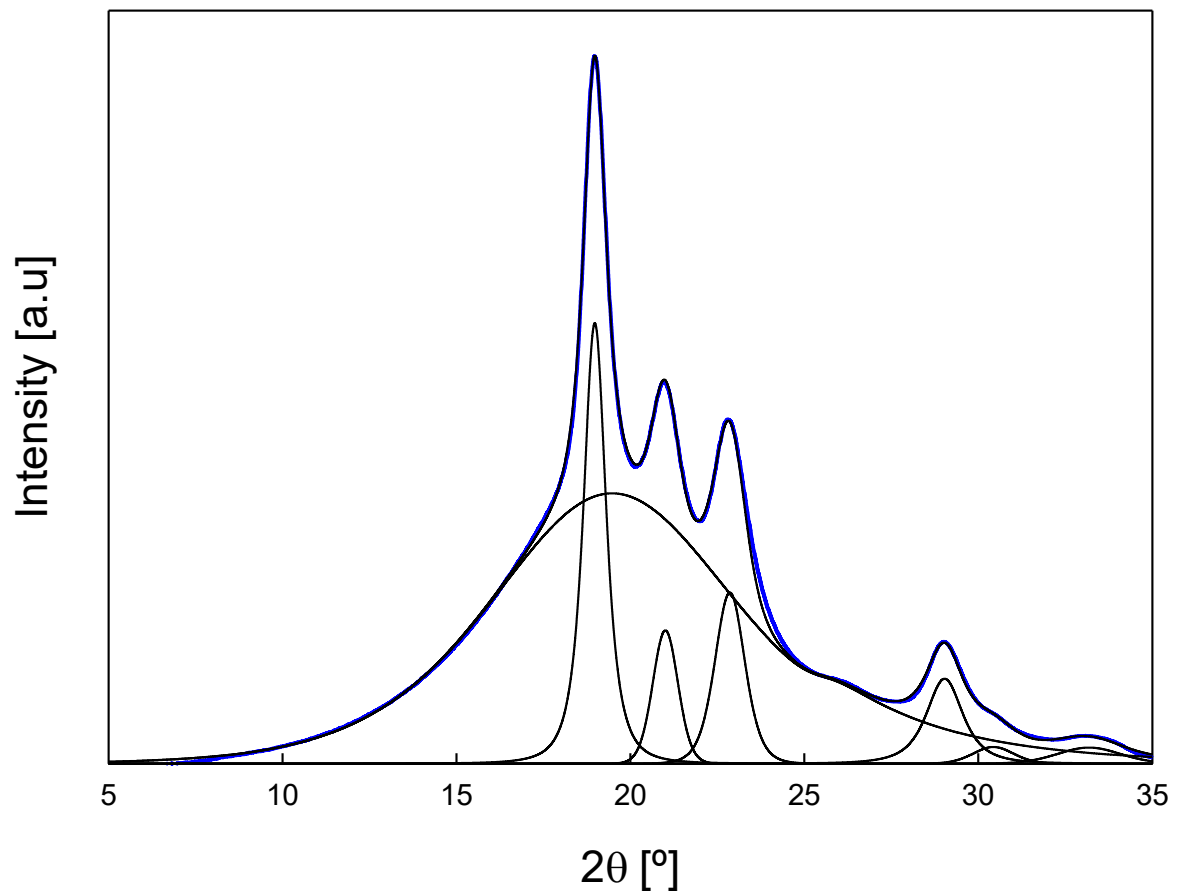


Figure 24. PEEK 166.1hN deconvolution

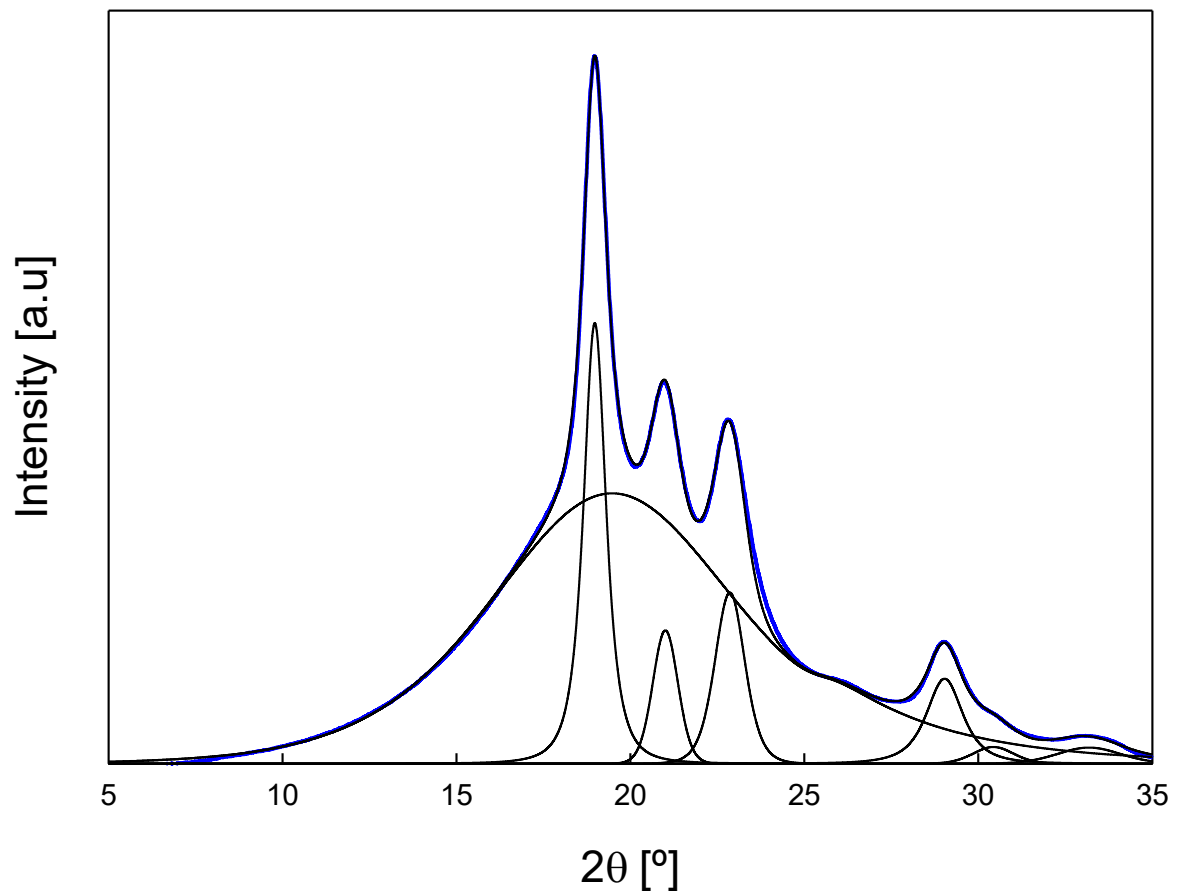


Figure 25. PEEK 240.1h deconvolution

The next figure represents the comparison between different samples.

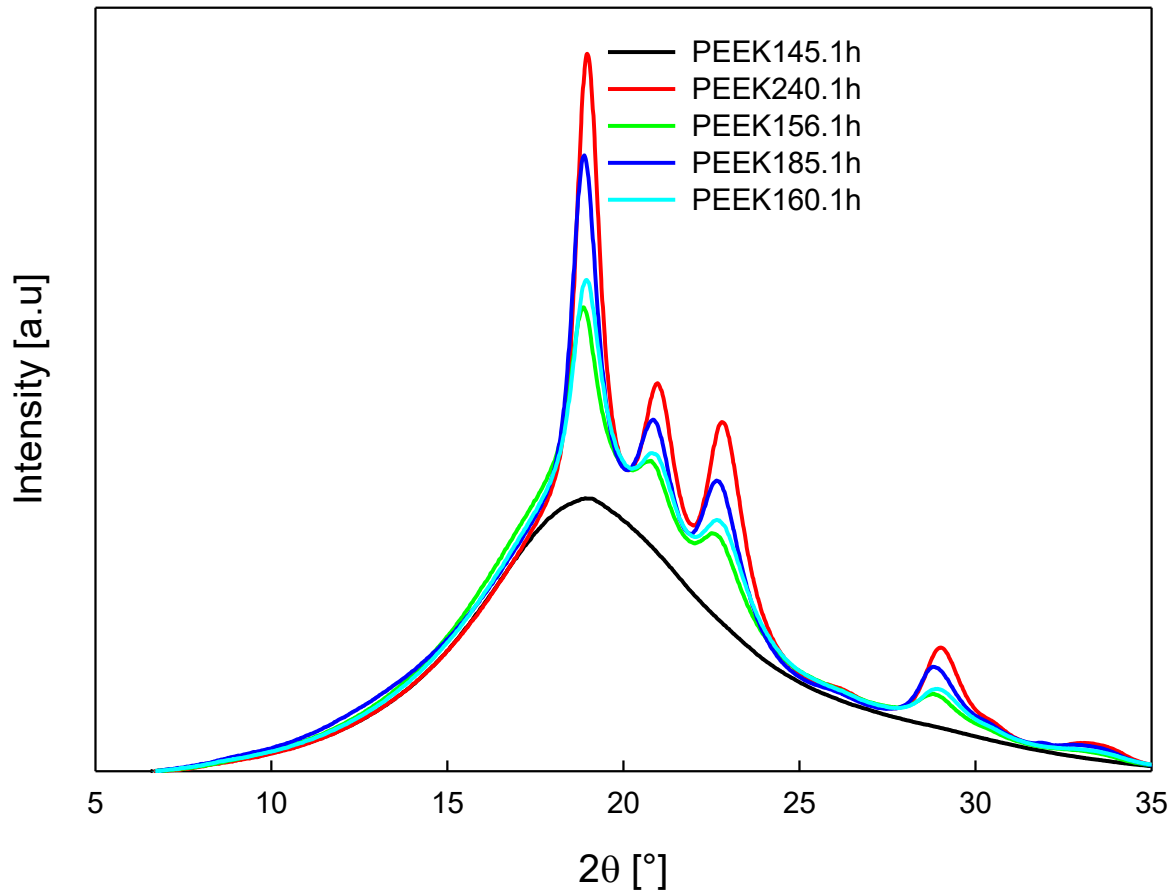
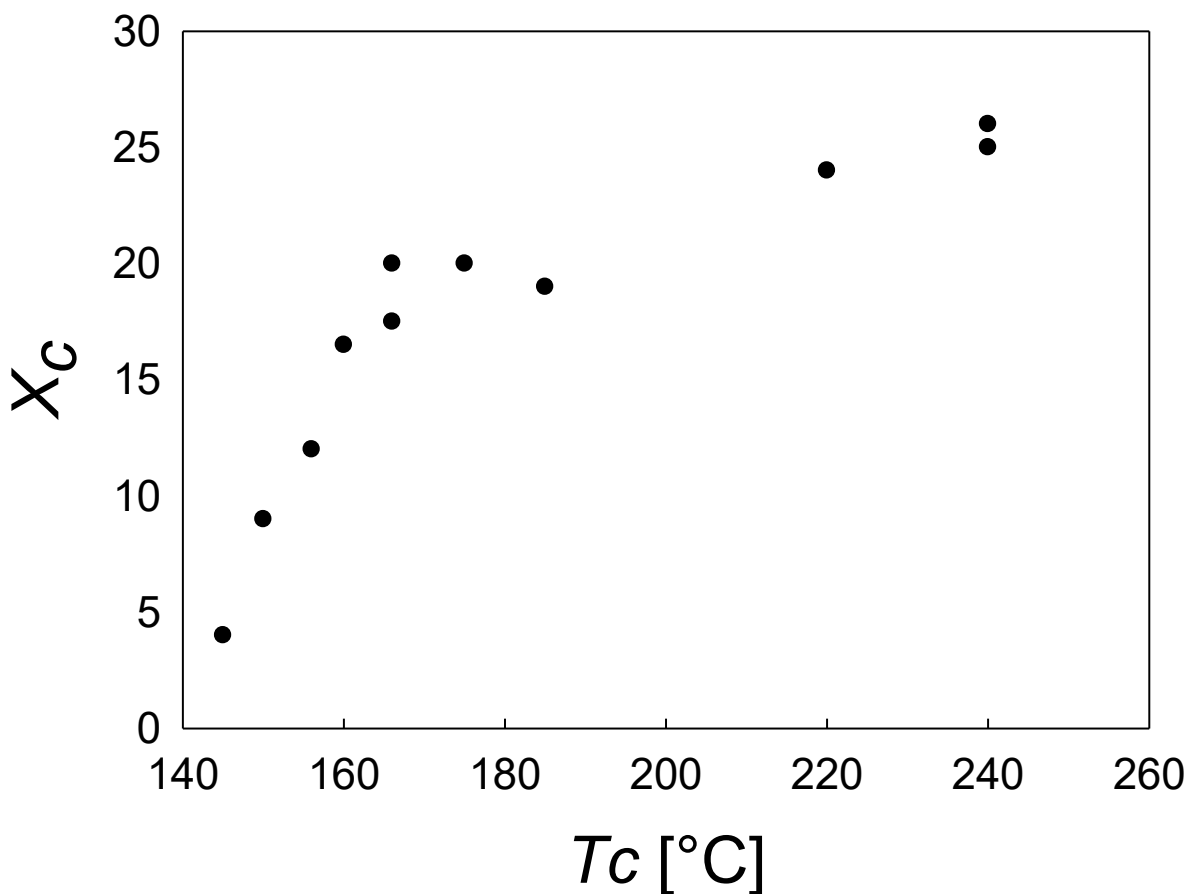


Figure 26. Comparison between different PEEK

The crystallinity seems to be a function of the crystallization temperature. The higher the temperature, the higher the crystallinity degree. This statement is confirmed with plot 4 showing the relationship between the crystallinity degree and the temperature at constant exposure time, 1 hour.

It can be seen that, with the cold crystallization conditions employed, the maximum crystallinity obtained is equal to 26%.



Plot 4. Crystallinity degree vs Temperature

In addition, it should be noted that a number of samples showed preferential crystal orientations. This can be easily detected by inspection of the diffraction patterns. In such cases, the distribution of intensity along the diffraction maxima is not homogeneous. This could be associated to situations in which the hot stage holder was tightened too much. Moreover, such samples also present the highest degrees of crystallinity probably because there was a good contact between the sample holder and the polymer films. To explore if a sample is isotropic or if it has preferential orientations it is necessary to do a plot of the intensity as a function of the azimuthal angle, centered around the diffraction maximum of interest. For instance, Figure 27 shows that the PEEK166.1h sample exhibits preferential orientation because the intensity plot as a function of azimuthal angle exhibits maxima and minima for different crystalline planes.

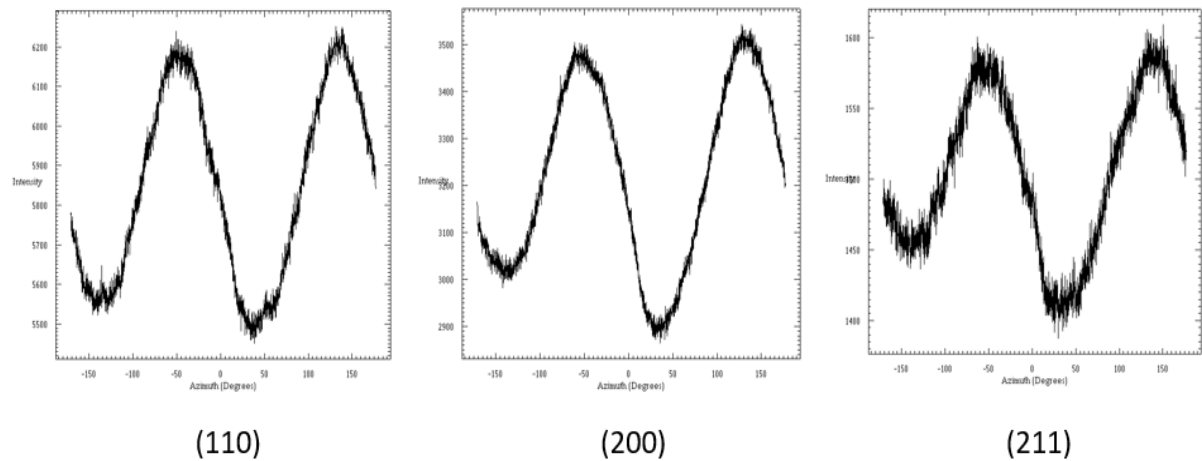


Figure 27. PEEK166.1h orientation planes

To better understand this aspect, the three plots of Figure 27 have been represented in Figure 28. As we can see the plane (110) in black, the plane (200) in red and the plane (211) in blue suggest orientation because there is a sequence of maxima and minimum with relatively low noise.

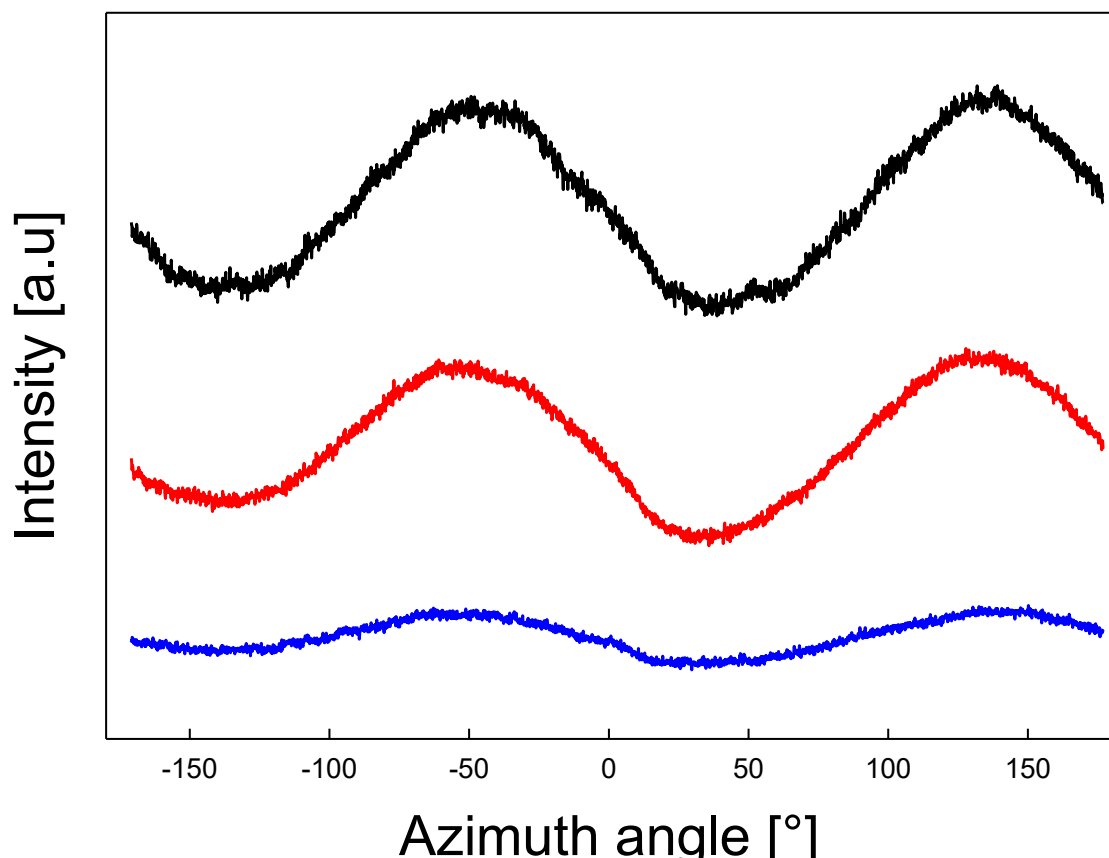


Figure 28. Preferential orientation of PEEK166.1h with tight ends

Finally, the table below divides the samples in isotropic or with preferential orientations.

Table 4. Isotropic and anisotropic samples

Isotropic samples	PEEK with preferential orientations
PEEK150.1h	PEEK166.1h
PEEK160.1hN	PEEK156.12h
PEEK156.1h	PEEK220.1h
PEEK160.1h	PEEK166.12h
PEEK166.1hN	PEEK175.1h
PEEK240.1h	
PEEK240.1hN	
PEEK145.1h	
PEEK185.1h	

3.1.1.1 Grain size calculation

With the Scherrer equation (2.1), we are able to calculate the dimension of the grain size. This calculation is important because the bigger the grain the higher the mechanical properties can be expected. The following tables show the grain size dimension of the different samples.

Table 5. PEEK grain size

Sample	(110) Å	(111) Å	(200) Å	(211) Å	(020) Å
Isotropic Samples					
PEEK145.1h	36	-	-	-	-
PEEK150.1h	97	112	82	59	68
PEEK185.1h	112	117	92	69	62
PEEK156.1h	96	101	100	56	45
PEEK160.1h	102	115	87	55	40
PEEK240.1hN	116	106	88	76	52
PEEK240.1h	118	106	89	74	67
PEEK166.1hN	105	104	85	74	76

Samples with preferential orientations					
PEEK156.12h	104	106	81	63	47
PEEK220.1h	118	106	91	74	67
PEEK175.1h	107	104	88	63	50
PEEK166.12h	108	108	90	60	50
PEEK166.1h	115	104	87	82	55

3.1.2 Mechanical properties from nanoindentation

As above mentioned in the Materials and methods section, the mechanical properties of the samples are determined using a nanoindenter G200. The temperature inside the nanoindenter cabin is controlled by a thermocouple: in this case it is fixed between 27-28°C. Table 6 shows the main properties of the materials: the hardness and storage modulus. Depending on the crystallinity, the storage modulus ranges from 3.70 GPa to 4.30 GPa, and the hardness varies from 260 MPa to 330 MPa.

Table 6. Mechanical properties and degree of crystallinity for the PEEK samples.

Sample	Orientation	Crystallinity	E' (GPa)	H (MPa)
Isotropic Samples				
PEEK150.1h	-	9%	3.84±0.06	264±7
PEEK156.1h	-	12%	3.88±0.05	271±5
PEEK240.1h	-	26%	4.44±0.03	332±6
PEEK160.1h	-	16.5%	3.79±0.08	263±9
PEEK185.1h	-	19.5%	4.27±0.08	312±6
PEEK166.1hN	-	17.5%	4.12±0.05	294±6
PEEK145.1h	-	4%	3.28±0.05	201±7
PEEK240.1hN	-	25%	4.27±0.04	307±9
Samples with preferential orientations				
PEEK166.1h	(110) (200) (211)	21%	4.26±0.03	306±5
PEEK156.12h	(110)	19%	4.11±0.06	297±5

PEEK220.1h	(110) (200)	24%	4.39 ± 0.06	329 ± 8
PEEK166.12h	(110) (200)	20.5%	4.21 ± 0.07	309 ± 8
PEEK175.1h	(110)	20%	4.18 ± 0.05	305 ± 6

The data in table 6 indicate also that preferential orientation does not affect the mechanical properties.

In order to gain a deeper understanding on the mechanical behavior of these PEEK samples, figure 29 illustrates the storage modulus as a function of the indenter displacement whereas figure 30 shows the hardness values as a function of the indenter displacement for samples without preferential orientations. [11]

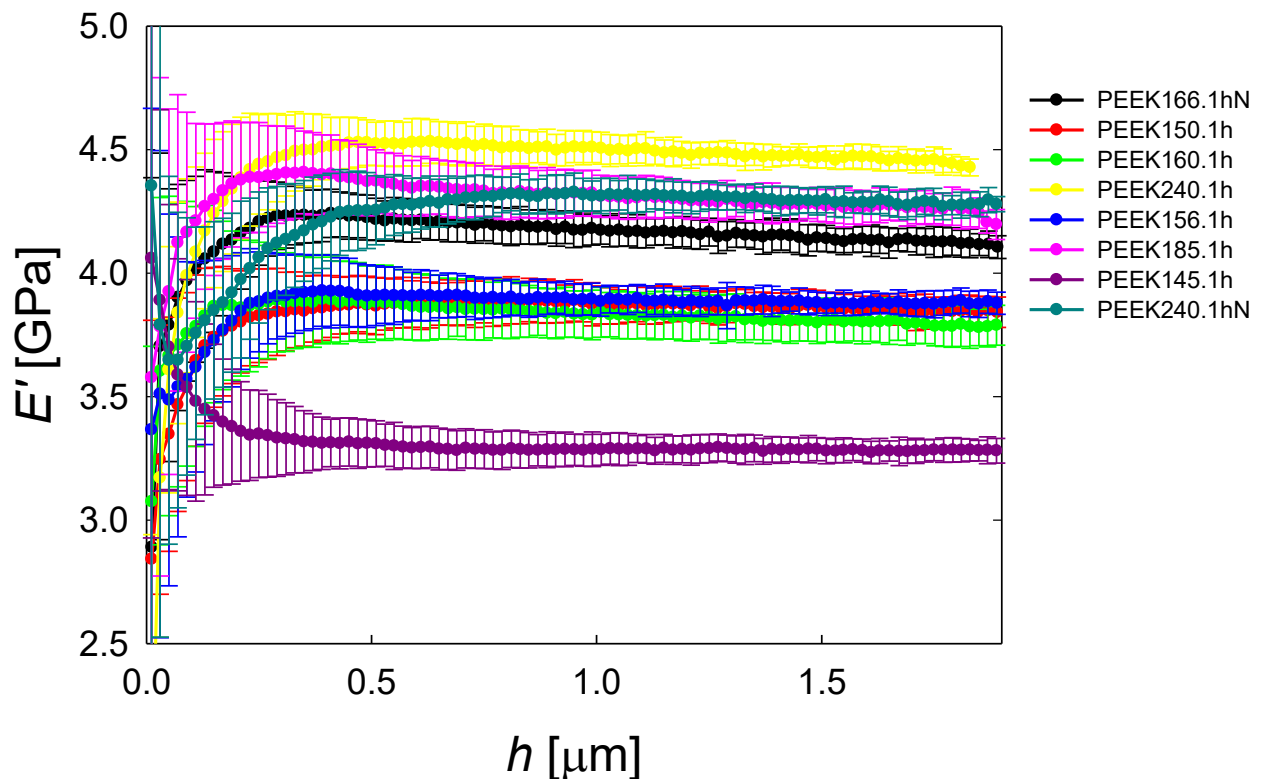


Figure 29. E' vs displacement, h

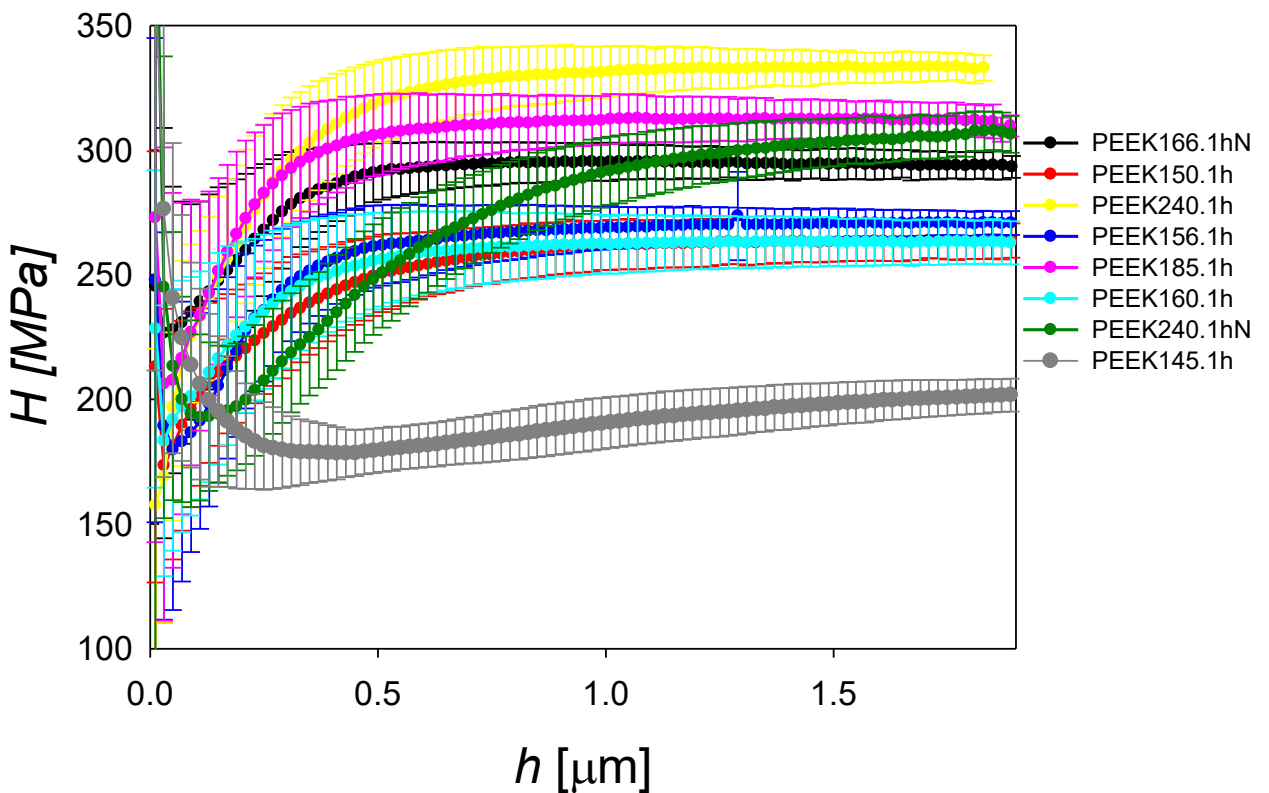
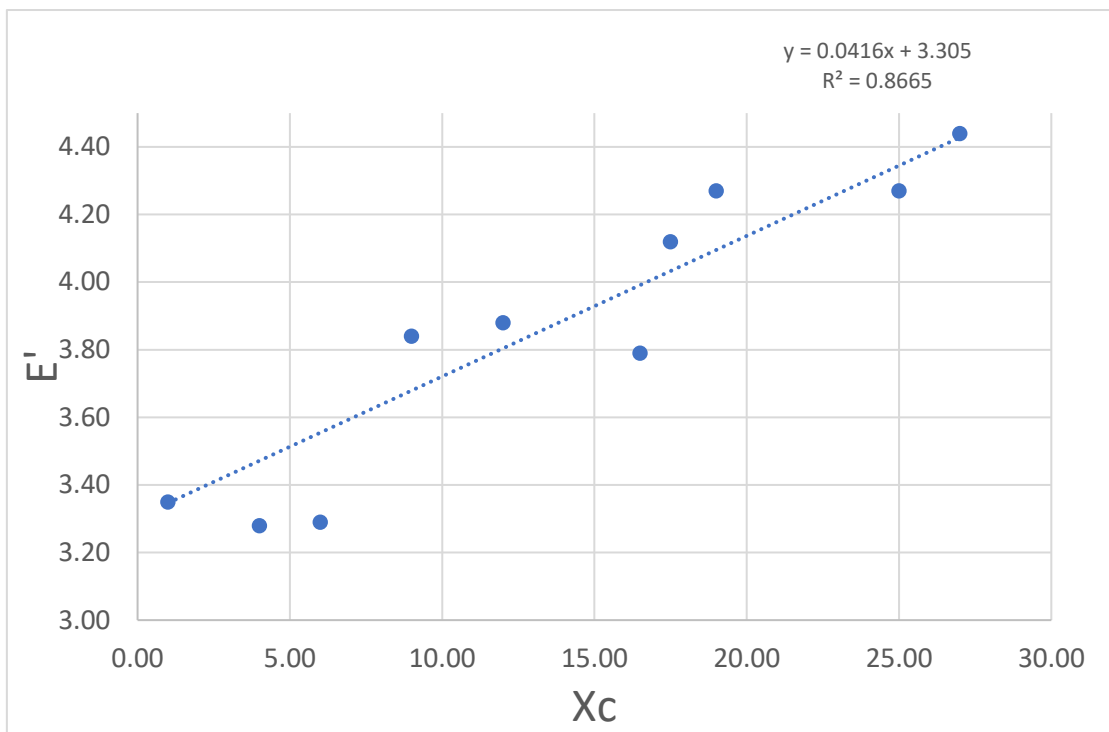


Figure 30. Hardness vs displacement, h

The error bars are associated to the standard deviation arising from the statistical analysis of the 22 indentations produced at different locations of the sample. The improvement of the mechanical properties at low displacement (less than $0.5\mu\text{m}$) is due probably to the sample's roughness and to the inaccuracy of the contact tip-area. During the cold crystallization process it is possible that the sample is not homogeneously heated. As a consequence, an inhomogeneous morphology may arise and this can lead to a big dispersion of mechanical properties. However, the present results suggest that this can be disregarded because hardness and storage modulus show small error bars and kept themselves constant with the indentation depth. [12]

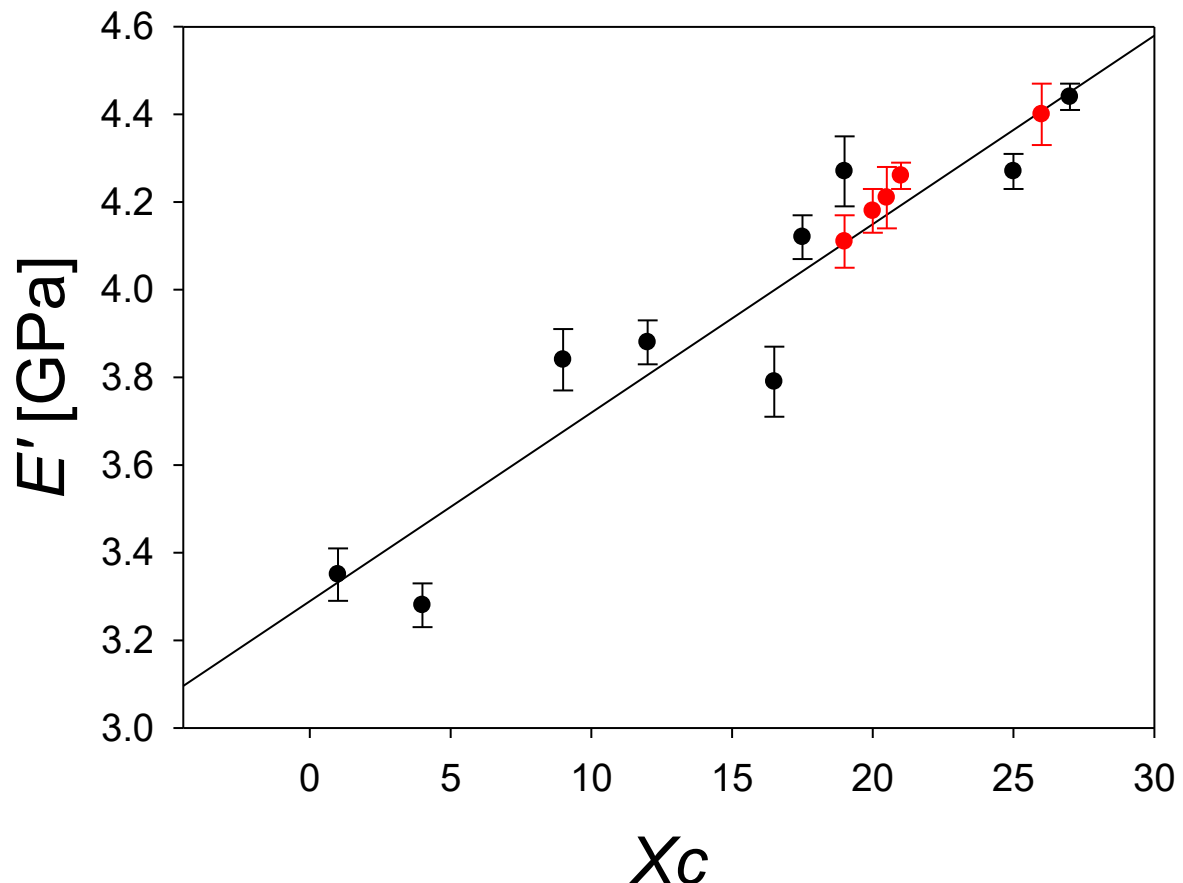
3.1.3 Correlation mechanical properties-crystallinity

Graphic 3 shows the storage modulus as a function of the degree of crystallinity for the different samples without preferential orientations. One can expect a linear relationship between the indentation mechanical properties and the crystallinity degree, as mentioned in the Materials and Methods part. In fact, the data of Graphic 3 show that the storage modulus is closely linked to the degree of crystallinity and there seems to be a fair linear dependence.



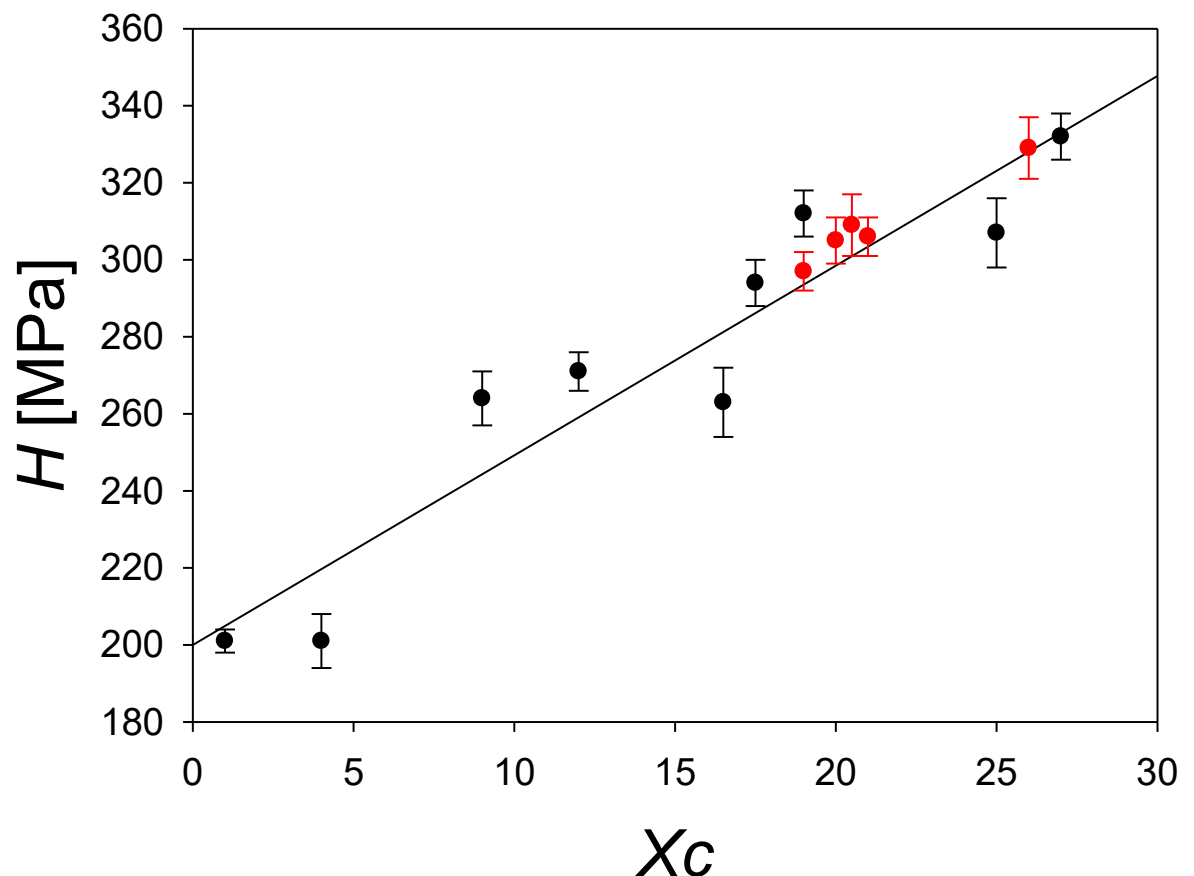
Graphic 3. Relationship between storage modulus and crystallinity degree

On the other hand, plot 5 includes data for PEEK samples with preferential orientation and without it. The first ones are represented in red and seem to fit perfectly well to the linear plot arising from the distribution of the isotropic samples (in black).



Plot 5. Storage modulus vs X_c for PEEK with preferential orientation, in red, and without preferential orientation in black.

Plot 6 illustrates a parallel analysis carried out with the hardness values as a function of the crystallinity and shows a similar dependence.



Plot 6. Relationship between hardness and X_c

It is found that the hardness and the storage modulus follow almost the same behavior with the degree of crystallinity.

3.2 Composites materials

3.2.1 Influence of graphene on PEEK properties

In order to explore the local mechanical behavior of the PEEK composites, nanoindentation was used. One of the goals of this work is to analyze and compare the results between the mechanical properties of PEEK without filler, PEEK with graphene and the latter as part of multilaminar system with CF fabric. As aforementioned, the PEEK composites analyzed are three:

- PEEK+CF1
- 5GsPEEK
- PEEK+CF3Gs

Figure 31 shows the 2D WAXS pattern of the 5GsPEEK nanocomposite (thickness equal to 480 μm). The intensity distribution along the azimuth for the (110) and (200) planes suggest preferential orientation and the crystallinity degree is 35%.

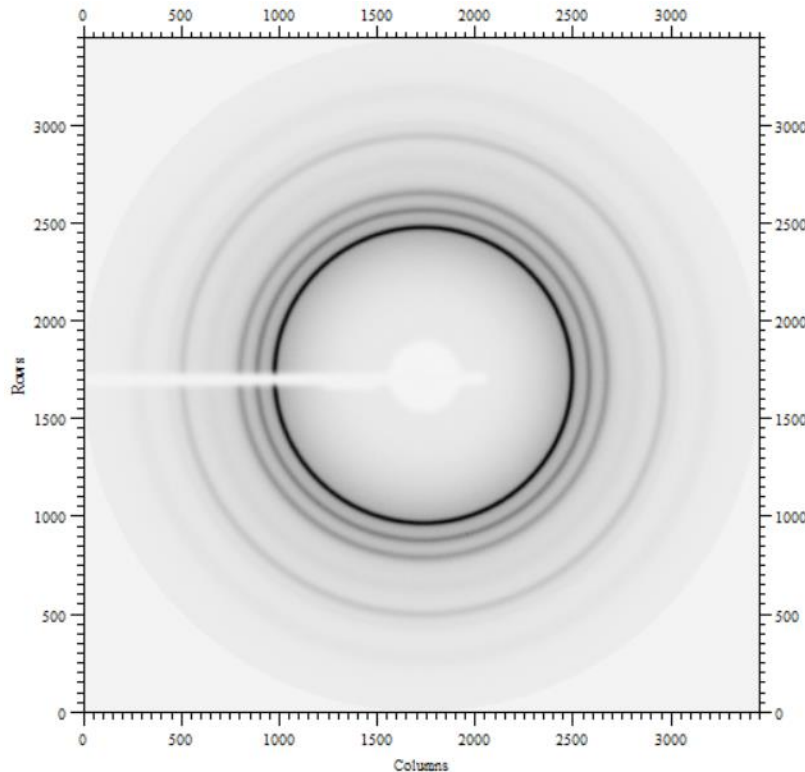


Figure 31. 5GsPEEK diffraction pattern

The same portion of the 5GsPEEK film was first used for X-ray measurements and afterwards embedded in epoxy resin for nanoindentation analysis. Nanoindentation data showed that the values of hardness and storage modulus for 5GsPEEK are higher ($E' = 6.3 \pm 0.1$ GPa and

hardness is 420 ± 20 MPa) than the ones for neat PEEK. Figure 32 represents the variation of the storage modulus with the displacement.

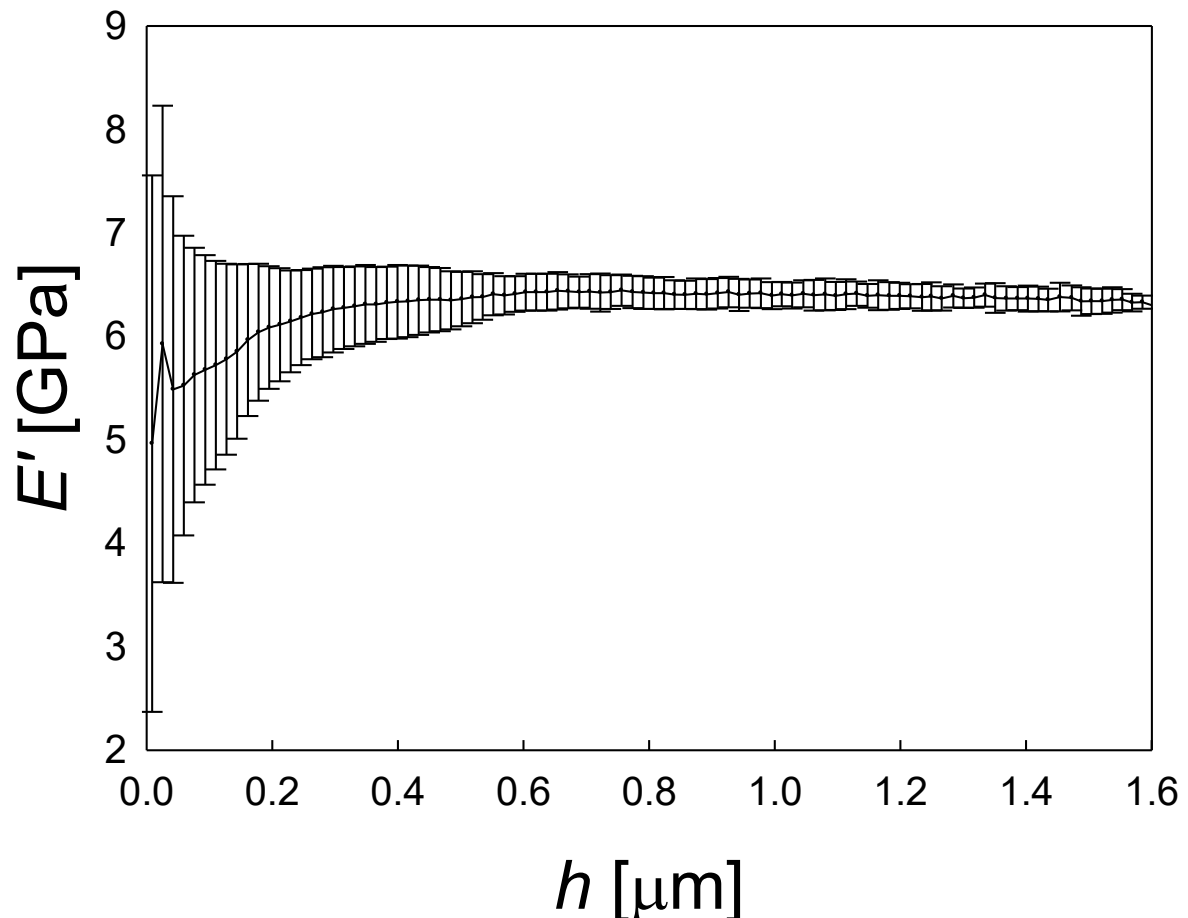
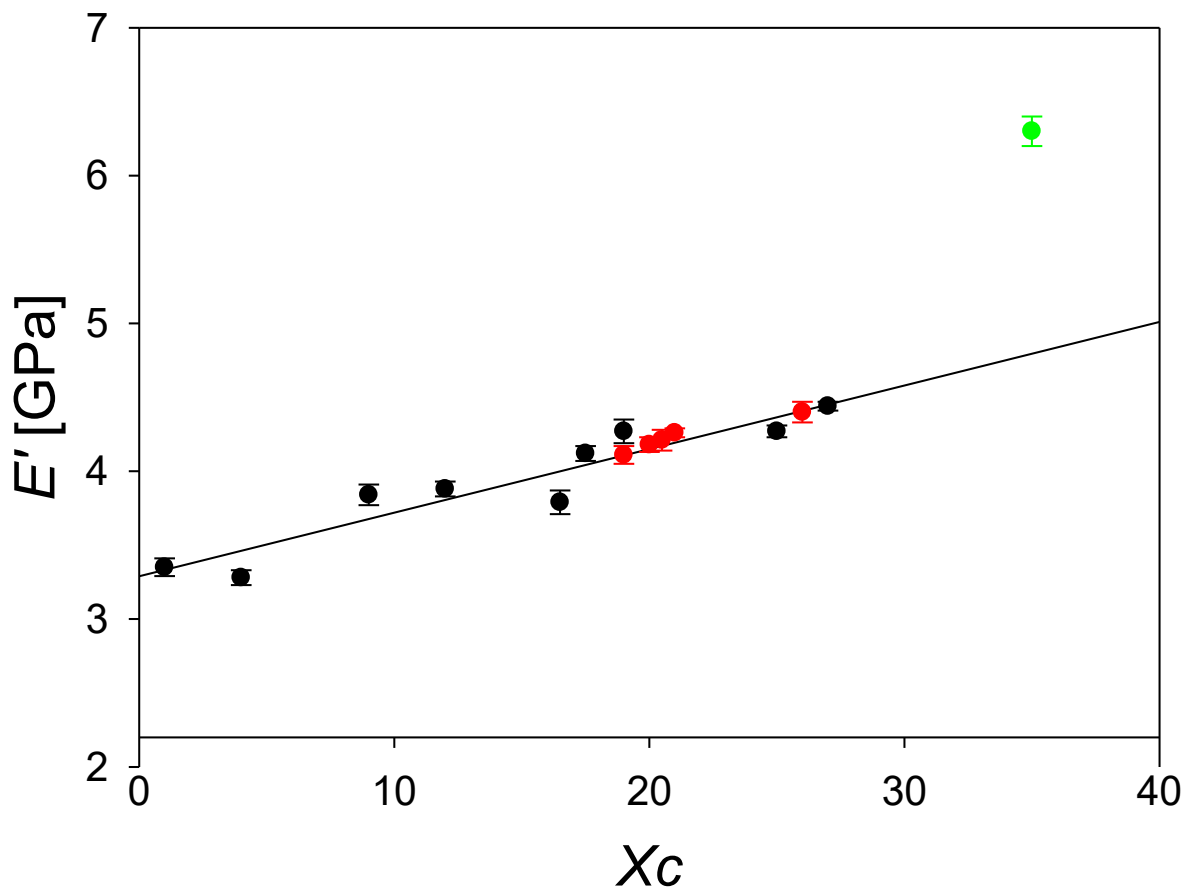
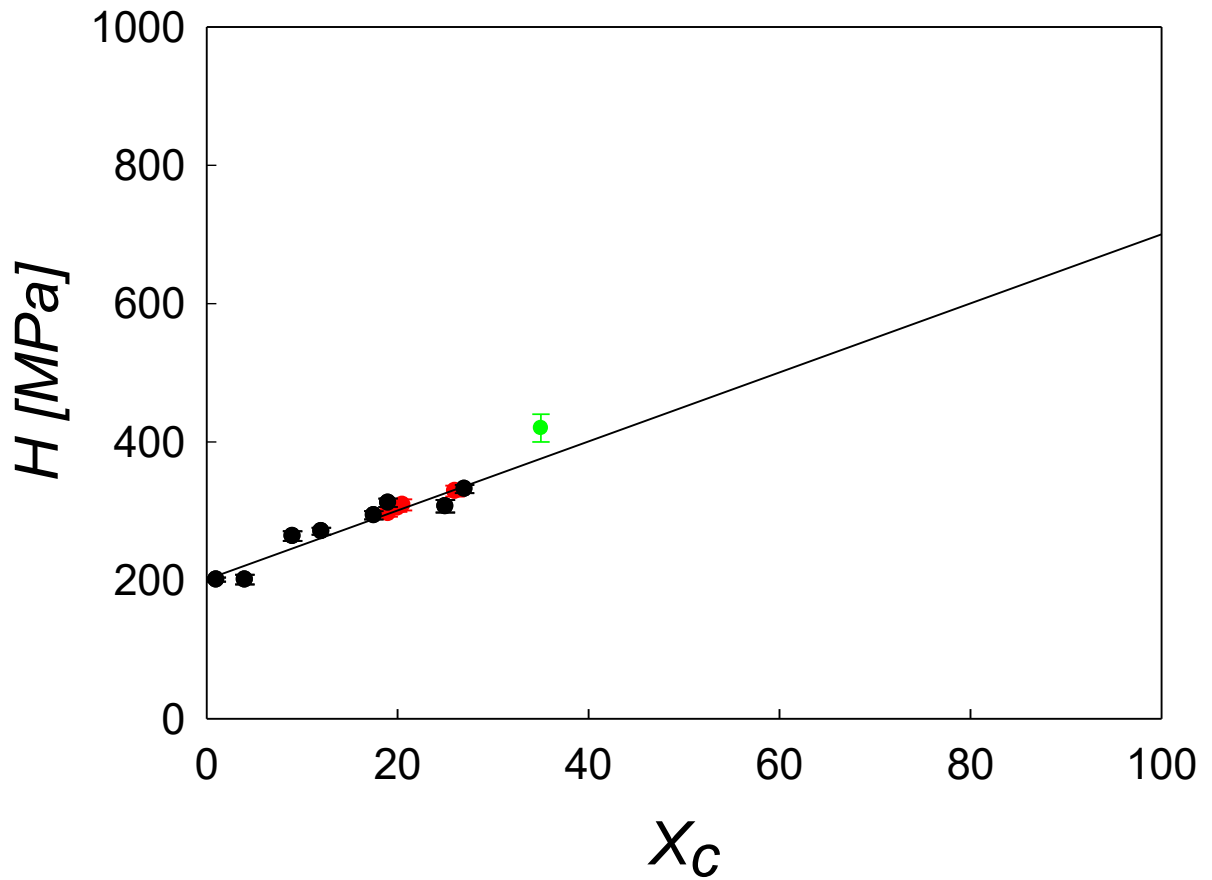


Figure 32. E' vs Displacement for 5GsPEEK

Plot 7 includes the E' values vs. X_c for neat PEEK without preferential orientation (black symbols); neat PEEK with preferential orientation (red symbols) and finally PEEK with 5% of graphene and preferential orientation (green symbols). According to what was discussed above, a linear relationship exists between E' and crystallinity degree. For a sample with the 35% of crystallinity and with approximately the same grain size we can predict that its storage modulus is equal to 4.8 GPa. However, we obtain $E' = 6.3 \pm 0.1$ GPa. Hence, the difference between these two values is due to the incorporation of the nanofiller. In other words, even if the PEEK/graphene nanocomposite is the most crystalline of all materials, the analysis of Plot 7 suggests that the mechanical increase is mostly due to the graphene. Such mechanical enhancement is of $\approx 30\%$ for 5 wt.% of graphene.



Plot 7. Correlation of E' vs X_c between PEEK with different crystallinity and PEEK with 5% of graphene (green)



Plot 8. Correlation of H vs X_c between PEEK with different crystallinity and PEEK with 5% of graphene (green)

On the other hand, plot 8 represents hardness as a function of the crystallinity degree. It should be noted that the extrapolation of the straight line to $X_c = 100\%$ yields the average hardness values of the crystalline regions (H_c). It seems that there is a general linear dependence that describes the hardness of neat PEEK as a function of the degree of crystallinity. This suggests that the lateral crystal size is not relevant in this case and hardness can be described in terms of only the degree of crystallinity. In the case of the nanocomposite, it is found that the lateral crystal size is slightly higher than those for pure PEEK (see Table 7). However, it is not expected that this small increase should be relevant to the mechanical properties in the light of the general linear trend depicted in Plot 8. Hence, the deviation of the green data from the straight line seems to be attributed to the reinforcement of the filler.

Table 7. 5GsPEEK grain size

5GsPEEK	D, Å	λ, Å	FWHM	FWHM, rad	2θ	θ rad
(110)	160	1.54	0.56	0.01	18.94	0.17
(111)	127	1.54	0.71	0.01	20.98	0.18
(200)	107	1.54	0.84	0.01	22.97	0.20
(112)	58	1.54	1.56	0.03	26.20	0.23
(211)	109	1.54	0.84	0.01	29.10	0.25
(020)	122	1.54	0.75	0.01	30.38	0.27
(121)	130	1.54	0.71	0.01	33.10	0.29
(212)	130	1.54	0.71	0.01	33.72	0.29

In the following, the mechanical properties of the laminar composite will be described and compared with those of 5GsPEEK. It should be remarked that the multilaminar material could not be analyzed by X-ray because of the high absorption of the carbon fibre fabric.

3.2.2 Composites properties

The following table compares the mechanical properties of the PEEK+CF1 and PEEK+CF3 laminates. Results for the 5GsPEEK nanocomposite are included for comparison.

Table 8. Storage modulus and hardness of PEEK composites

Samples	E' (GPa)	H (MPa)
PEEK+CF1	5.07 ± 0.04	370 ± 12
5GsPEEK	6.3 ± 0.1	420 ± 20
PEEK+CF3	6.6 ± 0.3	410 ± 20

These results are obtained based on 22 indentations performed on different areas of the sample: in the edges, in the center and between the carbon fibers. In this case, the indentations size approached the micrometer regime because the goal was to determine average values of the reinforced PEEK matrices. As an example, Figure 33 shows one indentation carried out between the fibre tows. The results in the table are the average.



Figure 33. Example of internal footprint; the fibers are they are aligned at 90° or 0°

The red circle highlights the footprint generated by the nano- indenter.

At first sight it seems that one arm of the indentation is larger than the other two. However, when the indenter was dismantled and placed in another position, the same arm still appeared longer. Hence, it seems that this observation is a consequence of the illumination coming from the upper side.

To explore the possibility of the appearance of an interphase between the carbon fibres and the PEEK matrix, and the influence of graphene, a number of indents on a line which passes across one carbon fiber were carried out. In this case, small indentations were produced, having an indentation depth of only 50 nm. Indentations were separated 0.5 microns from each other. Experiments were done both in the neat polymer layer and in the graphene-reinforced one. The objective was to evaluate the change in the nanometric properties of PEEK near and far from the carbon fiber and to observe the possible presence of interphases. To carry out such experiments, firstly, a single fibre was selected. Figure 34 shows the line across which the mechanical properties of the PEEK1+CF sample were explored.

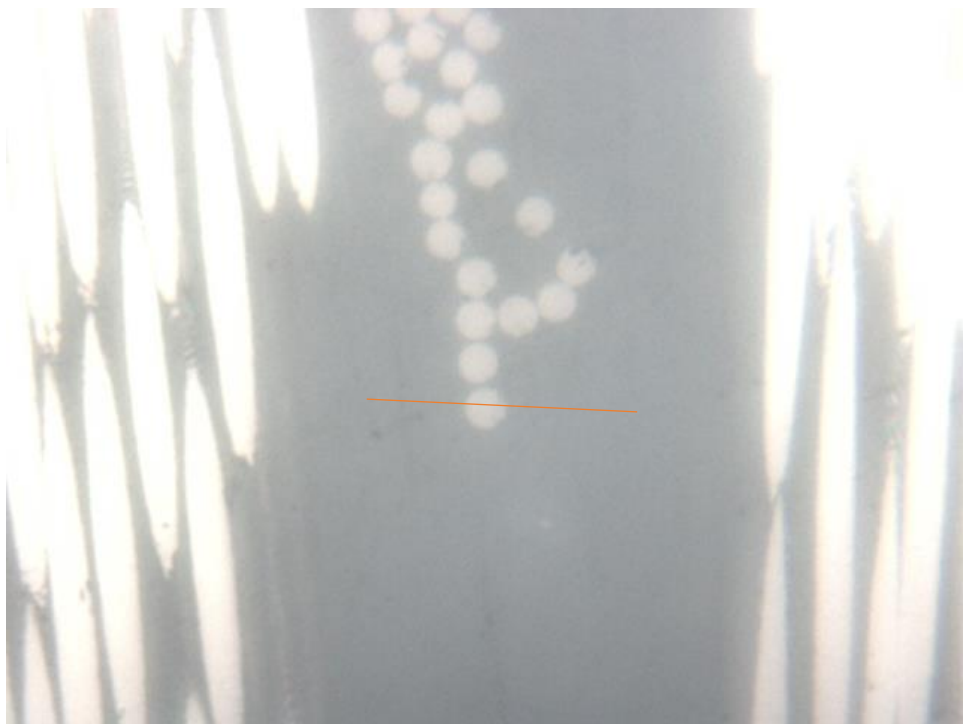


Figure 34. Indentation line

Figure 35 and 36 show the H and E' values, respectively, as a function of the distance of each indentation to the first one in the line.

PEEK+CF1

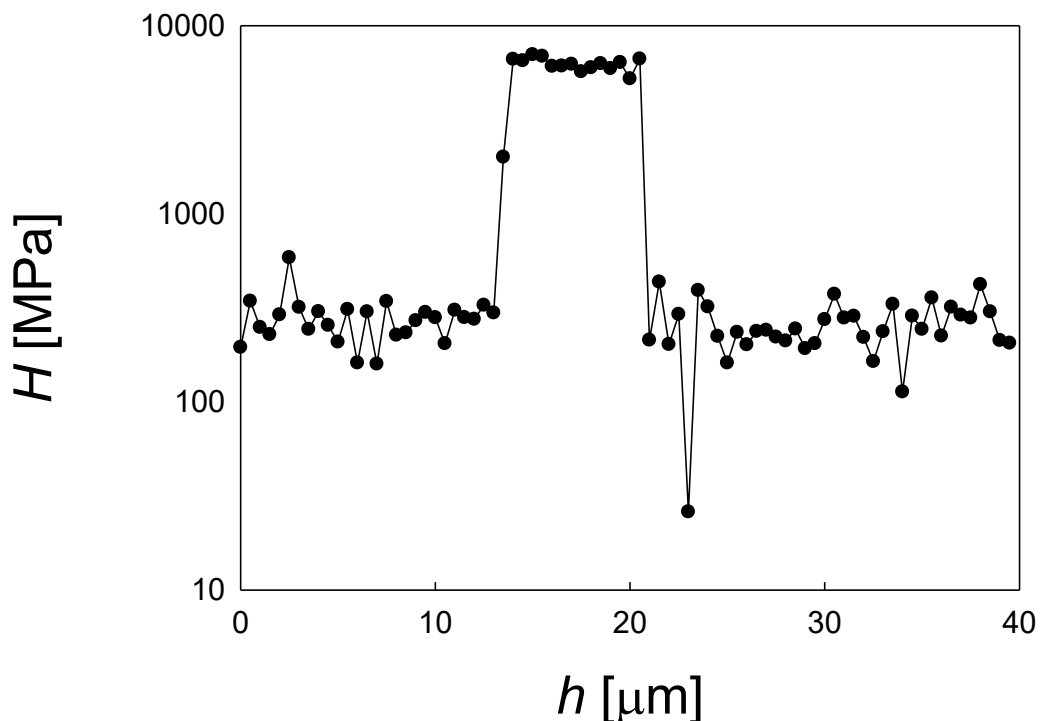


Figure 35. Relationship between H and displacement in PEEK+CF1

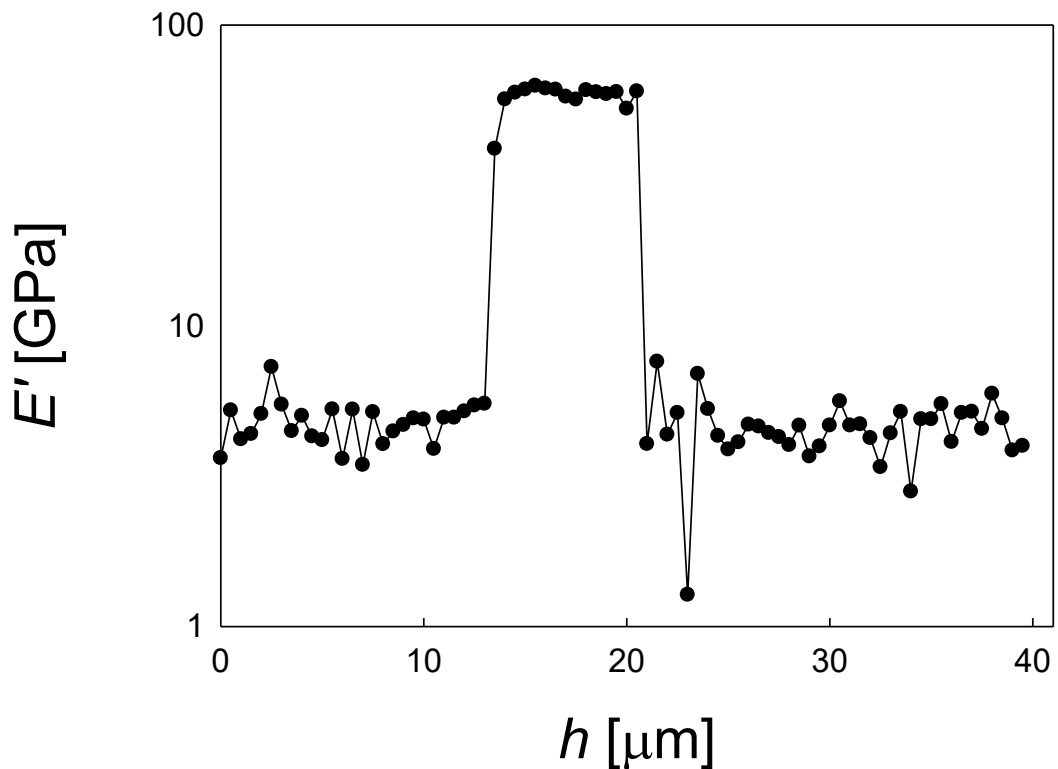


Figure 36. Relationship between E' and displacement in PEEK+CF1

As expected, indentations on the carbon fiber are associated to a drastic increase of the storage modulus and the hardness. Inspection of the data does not reveal the presence of an interphase. One cannot distinguish a region close to the fiber edge with distinct mechanical properties different from those of the PEEK matrix. Hence, it seems reasonable to attempt to promote such interphase by incorporating graphene to the polymer matrix.

PEEK+CF3Gs

Figure 37 and 38 show the results of a similar analysis carried out in the multilaminar system including graphene-reinforced layers. The graphene concentration in the PEEK layer is quite

low (\approx 5%).

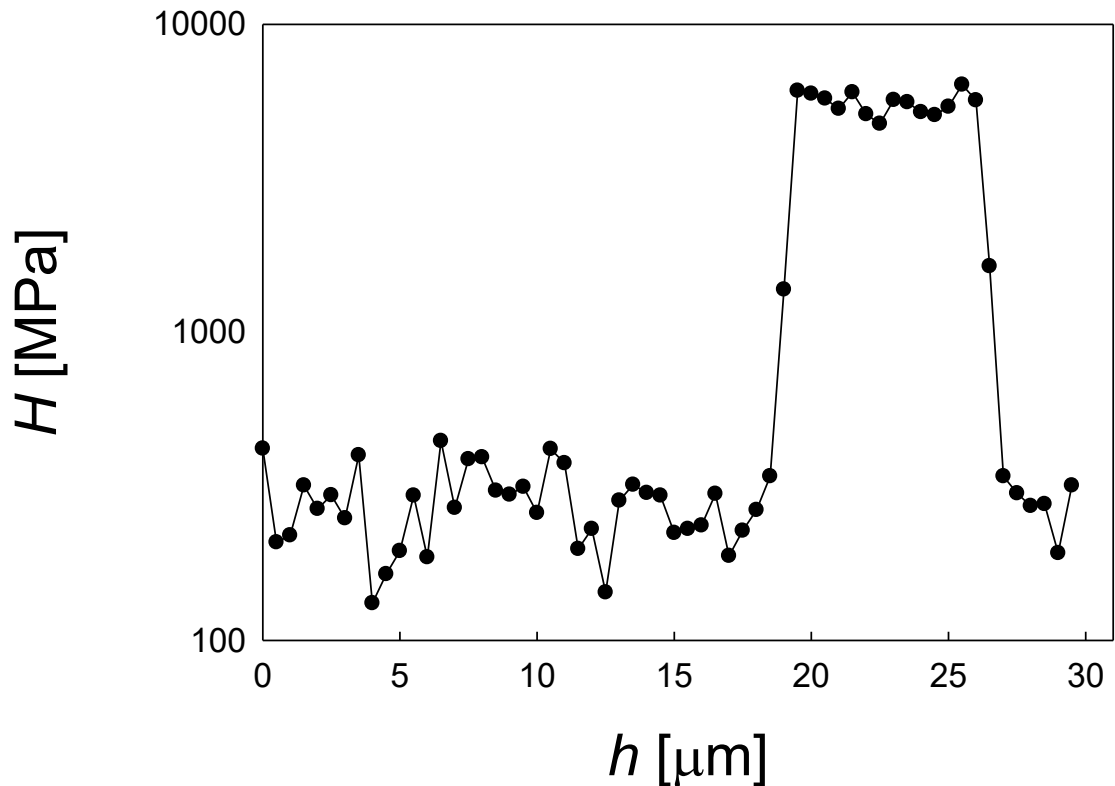


Figure 37. Relationship between H and displacement in PEEK+CF 3Gs

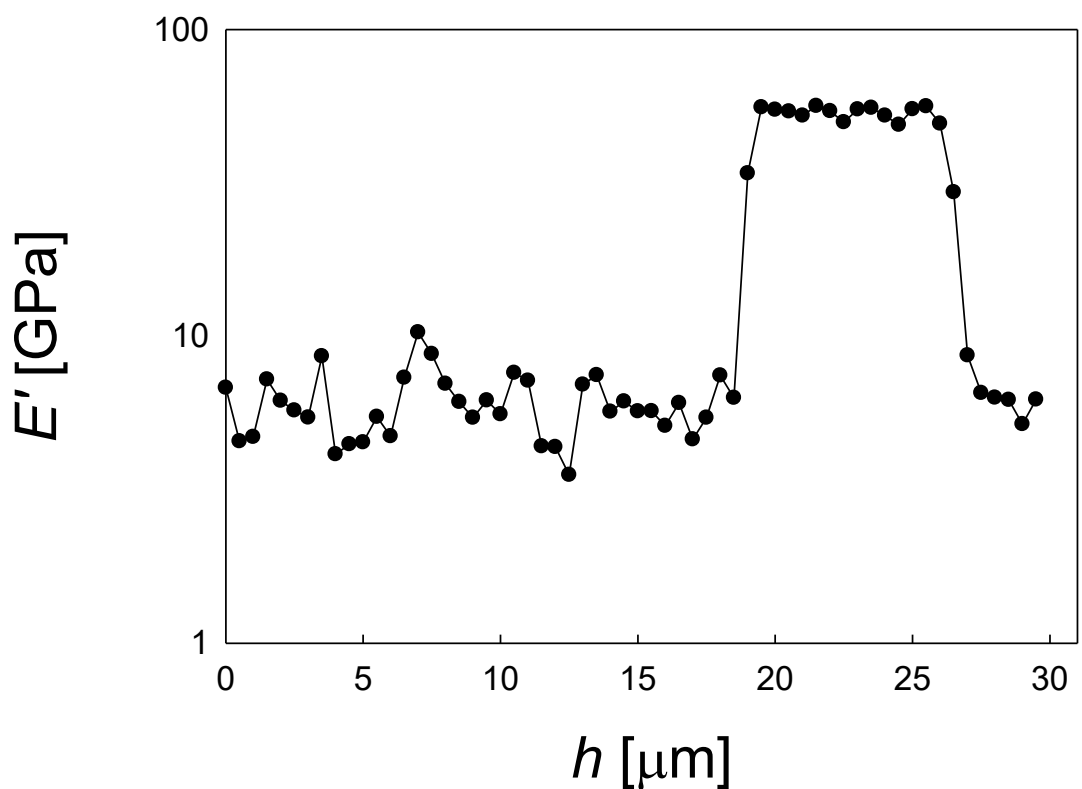


Figure 38. Relationship between E' and displacement in PEEK+CF3Gs

In this case, it seems that there is a slight increase of mechanical properties near the carbon fiber. However, such increase is quite small and it is not very well defined. Hence, with the present results, it is not possible to affirm that the addition of graphene leads to the formation of an interphase and therefore, a better adhesion between fiber and matrix. Further studies are needed, perhaps increasing the amount of graphene, or modifying the carbon fibres surface.

4. Conclusions

It has been shown that nearly amorphous PEEK can be transformed into a semicrystalline material by annealing at temperatures in the range 145 – 240 °C . It is found that by increasing the crystallization temperature, the degree of crystallinity is increased and there is a concurrent enhancement of modulus and hardness. A linear relationship between hardness (or modulus) with the degree of crystallinity is found. Moreover, changes in the size of the lamellar crystals in the range 3-12 nm have no relevant effect on the mechanical properties.

The incorporation of graphene produces a notable increase of mechanical properties (%5 in volume of graphene increase considerably the modulus and the hardness). Analysis of H and E' as a function of displacement into the surface suggests that graphene is well dispersed in the PEEK matrix at the micrometre scale. Analysis of the data, on the basis of the preceding established correlations between H (and E') and crystallinity, reveals that the nanostructural changes produced on PEEK by the incorporation of graphene do not significantly influence the mechanical properties. Hence, the major reinforcement is due to the intrinsic properties of the filler.

Concerning the multilaminar system, results did not show evidence of the occurrence of an interphase, neither in the neat polymer layer, nor in the graphene-reinforced one. A mapping of H and E' across the matrix-fibre interface did not show an apparent increase of mechanical property as the fibre edge was approached.

In summary, it has been found that graphene increases the hardness and modulus of PEEK. However, it does not seem to improve the interphase with the carbon fibres and hence, it is not expected that adhesion between them is improved. Hence, the incorporation of well-dispersed graphene is not enough to solve the problem of the interlaminar failure. Using a higher amount of graphene does not seem a suitable alternative because the filler is too expensive, and, in addition, agglomeration can be expected. Future work should consider other approaches such as modification of the surface of the carbon fibres in order to increase the wettability.

5. *Bibliography*

- [1] <http://www.miltonplastics.com/index.php/Picture/show/10.html>
- [2] Andrew J. Lovinger and D.D. Davis, Solution crystallization of PEEK, *Macromolecules* 19 (1986), 1-7.
- [3] Satish Kumar, David P. Anderson, W. Wade Adams, Crystallization and morphology of PEEK, *Polymer*, Volume 27, March 1986, 329-336
- [4] Victrex, 2013 Meeting the weight challenges of aircraft construction
- [5] Chris Velisaris and James Seferis, Crystallization Kinetics of Polyetheretherketone (PEEK), *Polymer engineering and science*, 1986, Vol.26, 22
- [6] Peggy Cebe, 1988, Annealing study of poly(etheretherketone), *Journal of materials science* 23 (1988) 3721-3731
- [7] Dimitri A. Ivanov, Roger Legras, and Alain M. Jonas, Interdependencies between the evolution of amorphous and crystalline regions during isothermal cold crystallization of poly(ether-ether-ketone), *Macromolecules* (1999), 32, 1582-1592
- [8] Amir Keyvan, Edalat Nobarzad, Mahdi Masoumi Khalilabad, Keivan Heirdari, 2014, Phase identification by X-ray diffraction
- [9] J. Hay, Introduction to instrumented indentation testing, Experimental technique, *Nanomechanical Characterization of Materials by Nanoindentation Series*, 2009
- [10] Ana M. Díez-Pascual, Marián A. Gómez-Fatou, Fernando Ania, Araceli Flores, Nanoindentation in polymer nanocomposites, *Progress in Materials Science* 67 (2015) 1-94.
- [11] S. Quiles-Díaz, P. Enrique-Jimenez, D.G. Papageorgiou, F. Ania, A. Flores, I.A Kinloch, M.A. Gómez-Fatou, R.J. Young, H.J. Salavagione, Influence of the chemical functionalization of graphene on the properties of polypropylene-based nanocomposites, *Composites:Part A* 100 (2017) 31-39.
- [12] Araceli Flores, 2017, Indentation in polymers, *Journal of Materials Education* Vol. 39 (5-6): 173-192 (2017)
- [13] J. Hay, P. Agee, and E. Herbert, Continuous stiffness measurement during nstrumented indentation testing, *Nanomechanical characterization of materials by nanoindentation series*, 2010.
- [14] Mark R. VanLandingham, John S. Villarrubia, Will F. Guthrie, and Greg F. Meyer Nanoindentation of Polymers
- [15] Xavier Tardif , Baptiste Pignon, Nicolas Boyard , Jürn W.P. Schmelzer, Vincent Sobotka, Didier Delaunay, Christoph Schick, 2014, Experimental study of crystallization of PolyEtherEtherKetone (PEEK) over a large temperature range using a nano-calorimeter, *Polymer Testing*, 36 (2014) 10–19
- [16] Federico Giuliano Nanoindentazione di film sottili di pedot: pss su substrato rigido, Università di Bologna
- [17] Alessandro Cinnirella Nanoindentazione dello strato di pentacene in OTFT sottoposti a irraggiamento ionico, Università di Bologna
- [18] Lin Jin, Jerry Ball, Tim Bremner, Hung-Jue Sue, 2014, Crystallization behavior and morphological characterization of poly(ether ether ketone), *Polymer* 55 (2014) 5255-5265

- [19] Luke Harris, 2011 A Study of the crystallisation kinetics in PEEK and PEEK composites, University of Birmingham
- [20] A. V. Fratini, E. M. Cross, R. B. Whitaker, W. W. Adams, Refinement of the structure of PEEK fibre in an orthorhombic unit cell, *Polymer*, 1986, Vol 27
- [21] http://www.xtal.iqfr.csic.es/Cristalografia/parte_02-en.html
- [22] A. A. Mehmet-Alkan and J. N. Hay, 1991, The crystallinity of poly(ether ether ketone), *Polymer*, 1992, Volume 33, Number 16, 3527-3530
- [23]
https://www.google.es/search?q=grafico+carico+spostamento+indentazione&source=lnms&tbs=isch&sa=X&ved=0ahUKEwiD5sGz3evaAhVGbRQKHX9eA8MQ_AUICigB&biw=1536&bih=686#imgrc=voHGJHNYB9kNJM
- [24] A. C. Fischer-Cripps, Nanoindentation, *Mechanical Engineering Series 1*, 2011
- [25] G.Zhang, H.Liao, H.Yub, V.Jic, W.Huangc, S.G.Mhaisalkarb, C.Coddeta, 2006, Correlation of crystallization behavior and mechanical properties of thermal sprayed PEEK coating, *Surface and coatings technology*, Volume 200, 6690-6695
- [26] Mohammed Naffakh, Marian A. Gomez, Gary Ellis and Carlos Marco, Thermal properties, structure and morphology of PEEK/thermotropic liquid crystalline polymer blends, *Polymer engineering and science*, 2006
- [27] A. J. Waddon, M. J. Hill, A. Keller, d. J. Blundell, On the crystal texture of linear polyaryls (PEEK, PEK and PPS), *Journal of materials science*, 22 (1987) 1773-1784
- [28] Alain Jonadlt and Roger Legras, PEEK Oligomers: A Model for the Polymer Physical Behavior, *Macromolecules* 1993, 26, 2674-2678
- [29] R. Indu Shekar, T. M. Kotresh, P. M. Damodhara Rao, Kamal Kumar, 2008, Properties of High Modulus PEEK Yarns for Aerospace Applications, *Journal of applied polymer science*, Vol. 112, 2497–2510 (2009)